The Rotational Centre of the Large Magellanic Cloud

Alma Bergström

Lund Observatory
Lund University

2022-EXA195

Degree project of 15 higher education credits
June 2022

Supervisor: Paul McMillan

Lund Observatory
Box 43
SE-221 00 Lund
Sweden

Abstract

The Large and Small Magellanic Clouds (LMC & SMC) are the two largest galaxies orbiting the Milky Way (MW). The interactions between them have affected the evolution of both galaxies. The interactions have affected the galaxies differently depending on how strong they have been. Tidal forces from the interactions are argued to have produced a stream of stars and gas called the Magellanic Bridge. Due to the population of stars being young in the Bridge it is concluded that the Bridge was formed of only gas which was stripped from the galaxies. The Bridge is one of the most prominent proof that there have been a few or several interactions between the Small and Large Magellanic Cloud.

In this thesis, we have looked at eight evolutionary phases of stars with different ages for the different phases. They cover a wide range of ages from very young to old stars. We looked at how their proper motion, rotational velocity, and rotational centres behave and what differences and similarities we can see between the stellar populations. This was done using three different models for the rotational and radial velocities where one of the models was used with masked and unmasked data. The rotation curve for each of the populations was derived as well as the internal velocities, the velocities within the LMC.

By fitting a model with a non-fixed centre we could determine the rotational centres for the stellar populations. These centres were compared to results of other authors. We find that the centres derived in this thesis are closer together than what was previously derived. We can therefore conclude that the interactions have affected the LMC less than what was previously theorised.

Populärvetenskaplig beskrivning

Galaxer formas när enorma gasmoln kollapsar på grund av gravitation. Små ojämnheter får gasen att rotera vilket leder till att molnet pressas ihop till en disk. Stjärnor bildas av gasen som i sin tur fortsätter att rotera. Under tid dör stjärnorna och blir till gas igen som sedan bildar nya stjärnor.

Interaktioner mellan galaxersker genom kollisioner och gravitationskrafter. Det kan påverka galaxerna genom externa krafter som ändrar positioner av gas och stjärnor. Eftersom stjärnor bildas av gas påverkas också stjärnformationen i galaxen. Interaktioner sker under lång tid och vissa är starkare än andra. Stjärnor påverkas därför olika mycket beroende på deras ålder. Rotationscentrum för de olika åldrarna av stjärnor kan därför vara skilda från varandra.

De Magellanska Molnen är två dvärggalaxer som åker i en omloppsbana runt Vintergatan. Detta gör dem till satelitgalaxer för Vintergatan. Det Stora Magellanska Molnet (LMC) och det Lilla Magellanska Molnet har interagerat både med varandra och med Vintergatan. Som bevis på detta har man observerat ett gas moln som sträcker sig från Vintergatan och binder samman dem två Magellanska Molnen, Magellanska Strömmen. Det är den mest studerade gasförbindelsen mellan två galaxer.

I det här arbetet kommer stjärnor i LMC av olika åldrar att analyseras med hjälp av data från rymdteleskopet Gaia. Datan kommer att användas för att hitta rotationskurvan för de olika stjärngrupperna, det vill säga hur snabbt stjärnorna i varje grupp roterar med avseende på radien, med hjälp av modeller som beskriver rotationshastigheten som funktion av radie. Genom att låta en av modellerna ha rotationscentrumet som en fri parameter kommer dessa centrum kunna bestämmas för var och en av stjärngrupperna. Med hjälp av detta kan vi utveckla kartläggningen av interaktionerna mellan de Magellanska Molnen genom tiderna.

Contents

Chapter 1

Introduction

Figure 1.1: The Magellanic Clouds. the Large Magellanic Cloud is visible in the upper right corner while the Small Magellanic Cloud is visible in the lower left part of the image. Picture credit: ESO/S. Brunier (27 August 2009).

1.1 The Large Magellanic Cloud

The Milky Way is located within the galaxy group the Local Group. Besides the Milky Way, there is another larger galaxy in the Local group, Andromeda and a number of dwarf galaxies. Two of these are the Small and Large Magellanic Clouds, which are satellite galaxies orbiting the Milky Way pictured in A.5. The Large Magellanic Cloud (LMC) is one of the biggest dwarf galaxies within the Local Group and the biggest orbiting the Milky Way (Wan et al. 2020).

The LMC is located at a distance of 50-60 kpc from the Milky Way (Bagheri et al. 2013), with the latest estimates being that it is 49.5 kpc from the Sun Pietrzyński et al. (2019). It is thought to have a mass of $1 - 2.5 \cdot 10^{11}$ $M_\odot$ (Erkal 2019), compared to the MW mass of 10^{12} $M_\odot$ (Cautun et al. 2020).

1.2 Gaia Telescope

A telescope in space can observe objects without the blurring effect of the Earth's atmosphere, unlike telescopes based on the ground. Gaia is a space based observatory, a mission of the European Space Agency (ESA) (Gaia Collaboration et al. 2016). It was launched in December 2013. Its operating point is the second Lagrange point of the system consisting of the Sun, the Earth and the Moon. The Gaia Collaboration provides open access to its data, with regular data releases Gaia Collaboration et al. (2021). The data is available from the Gaia archive on Gaia's Home page[1]. One of the Gaia Mission's scientific topics is the Local Group, including the Magellanic Clouds. By observing millions of stars in the Large Magellanic Cloud, the Mission aims to learn more about the Magellanic Clouds, the interaction between them and the interaction between the Clouds and the Milky Way (Gaia Collaboration et al. 2016).

1.3 Colour-Magnitude Diagram and Stellar Populations

Colour-Magnitude Diagrams show the number of stars observed as a function of their colour and apparent magnitude. A colour-magnitude diagram of the stars in the LMC is shown in figure 1.2 created with data from Gaia. The y-axis is the magnitude of the stars in the G-band (the Gaia-band). It is defined as an unfiltered white photometric band between the wavelengths 330 - 1050 nm. The x-axis is the difference between the Blue and the Red photometric bands. The Blue Photometric band (BP) is between 330-680 nm and the Red Photometric band (RP) is between 640-1050 nm (Gaia Collaboration et al. 2016). The stars are in different parts of the diagram depending on which evolutionary phase they are in. The peak to the left, $(G_{BP} - G_{RP}, G) \sim (0, 14)$ to $(0.5, 20)$, is the main sequence which consists of stars in their main phase of life and are considered young. Higher up in the diagram are the youngest stars while further down are the older, but still young, stars. The peak to the right, $(G_{BP} - G_{RP}, G) \sim (1, 20)$ to $(3, 16)$, which diverge is the Red Giant Branch in the first half while the second half is the Asymptotic Giant Branch.

[1] https://sci.esa.int/web/gaia

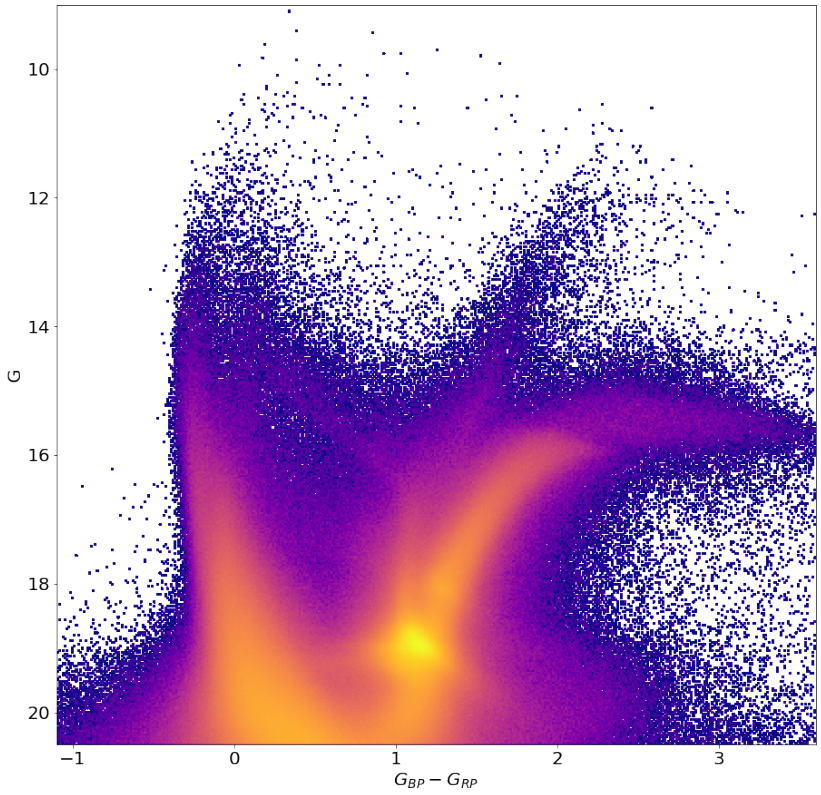

Figure 1.2: Colour-Magnitude Diagram of the data sample from the LMC.

1.4 Galaxy Interactions

An important part of galaxies evolution are interactions with other galaxies (Harris 2007). They can interact by colliding or interact through gravitational and tidal forces. The collisions can lead to mergers and the gravitational and tidal forces can lead to stripping of gas and stars from the galaxies. This could create stellar and gaseous streams and tails from the galaxies. The collisions can lead to either an increase or decrease of star formation.

One of the most studied gas streams is the Magellanic Bridge which was first detected by Hindman et al. (1963). The Magellanic Bridge was believed to have been created from stripped gas only since only young stellar populations were detected (Harris 2007). If older stellar populations could be detected within the Bridge, we would know that stars in addition to gas would have been stripped from the galaxies. Wan et al. (2020) argue that the tidal interactions between the clouds have induced an increase in star formation

in the Large Magellanic Cloud. This is because they found the rotational centres for the RGB and Carbon stars were closer together while the centre for the younger stars was distanced from them. The interactions have lead to the Magellanic Clouds having complex morphologies. These complex morphologies can be better explain by interactions between the two of them rather than gravitational interactions with the Milky Way (Besla et al. 2012).

1.5 This Project

This project has analysed data from the Gaia archive of objects within the LMC. The proper motion of the stars in the galaxy have been analysed for stars in different evolutionary phases. Several models were also used in order to analyse the radial and rotational velocity of the different evolutionary phases. The two first models that were used had a fixed centre of the LMC. Finally a model with the centre of the galaxy left as a free parameter was used in order to determine the rotational centre for each of the subsamples. The difference in dynamics of the evolutionary phases can provide information about the previous interactions between the Magellanic Cloud and the possible interactions between the Clouds and the Milky Way.

Chapter 2

Method

2.1 Obtaining the data

The data was selected through three steps. The first was through spatial selection. A base sample was collected from the Gaia archive, available on the Gaia web page[1]. The data for objects within a radius of 20° of the assumed centre $(\alpha_0, \delta_0) = (81.28°, -69.78°)$ (van der Marel 2001) were collected. We only selected stars brighter than G = 20.5. A sample with a total of 27,231,400 objects was obtained from the Gaia archive with the following ADQL query:

```
SELECT source_id, phot_g_mean_mag, ra, dec, parallax, parallax_error,
pmra, pmra_error, pmdec, pmdec_error, phot_bp_mean_mag, phot_rp_mean_mag,
parallax_pmra_corr,parallax_pmdec_corr,pmra_pmdec_corr,
dr2_radial_velocity, dr2_radial_velocity_error
FROM gaiaedr3.gaia_source
WHERE 1=CONTAINS(POINT('ICRS',ra,dec), CIRCLE('ICRS',81.28,-69.78,20))
AND phot_g_mean_mag<20.5 AND parallax IS NOT NULL
```

In the second step, the data was filtered using proper motion. The typical proper motion of objects in the LMC is different to the typical proper motion of the objects in the Milky Way. Foreground contamination was decreased using the proper motions of the two different galaxies. The numerical method requires to make a projection onto the tangent plane at (α_0, δ_0), using Eqn. 2 from Gaia Collaboration et al. (2021). This is because the right ascension and declination are both given in degrees but as we go further from $\delta = 0°$, $d\alpha$ becomes a smaller distance on the sky relative to an equal $d\delta$. Therefore Gaia Collaboration et al. (2021) define a two dimensional coordinate system which is a projection onto the tangent plane where

$$\begin{aligned} x &\simeq \cos(\delta)(\alpha - \alpha_c) \\ y &\simeq \delta - \delta_c. \end{aligned} \tag{2.1}$$

[1] https://gea.esac.esa.int/archive/

This coordinate system simplifies the calculations made later in the section.

To remove the foreground contamination a median proper motion of the LMC was determined. To do this:

- The sample was filtered by parallax $\varpi/\sigma_{\varpi} < 5$. This is to ensure that the distance to the objects in the sample is great enough for them to be in the LMC.
- Objects were filtered by radius such that $x^2 + y^2 < \sin(r_{sec})$, where $r_{sec} = 5°$. To determine the median proper motion a brighter magnitude limit was used, G=19.
- The median proper motion of the LMC was found from these objects to be $\mu_x = 1.854, \mu_y = 0.275$. We then determined the intrinsic spread of the proper motions, described by a covariance matrix. Objects within a 99% confidence region for this intrinsic speed were kept.

A final cut of the sample was done using proper motion, parallax and magnitude (G=20.5). The final sample contains 12,263,084 objects. The density on sky of the stars in the LMC using the sample is shown in Fig. 2.1. The LMC is mostly found within the inner 8 degrees. It shows features like spiral arms and a bar in the centre of the Cloud. The outskirts of the SMC can be seen towards the coordinates (-12,-12).

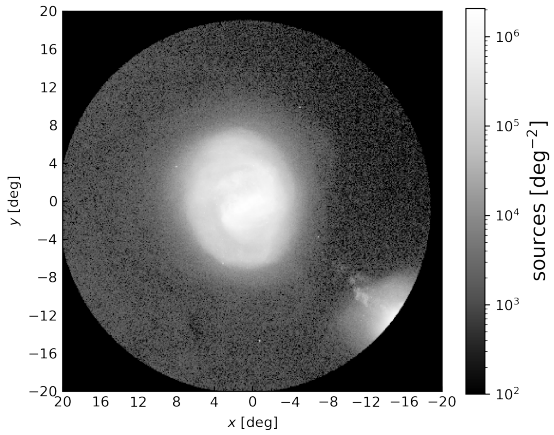

Figure 2.1: Density on sky of stars in the LMC of the final sample.

The result of the filtering of the sample is presented in the Colour-Magnitude diagrams in Fig. 2.2. The left CMD shows two peaks at $G_{BP} - G_{RP} = 1$ and all G magnitudes. which are not present after the sample have been filtered. The darker part under the asymptotic giant branch is partly removed by the filtering. The stars that are removed by the filtering are the Red Clump stars and the Main sequence stars in the Milky Way.

The last step in the selection of the sample was to divide it into eight sub samples. The sub samples were chosen based on the ages of the stars using the CMD of the stars in the

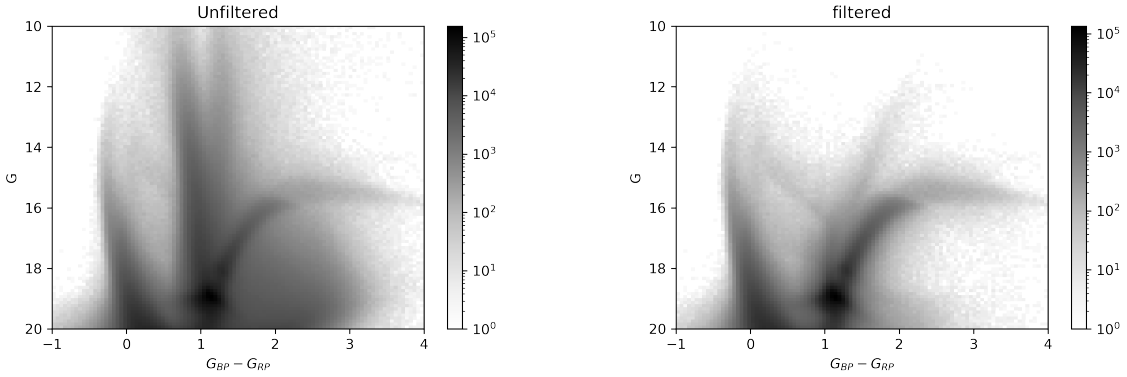

(a) Colour-Magnitude Diagram of the unfiltered data sample.

(b) Colour-Magnitude Diagram of the filtered data sample.

Figure 2.2

LMC. The eight sub samples therefore represents eight different evolutionary phases. The sub samples were chosen following the method in Gaia Collaboration et al. (2021) and the stars were divided into these sub samples. The CMD of the stars in the LMC with the eight evolutionary phases are shown in Fig. 2.4. The evolutionary phases are referred to as Young 1, Young 2, Young 3, RR-Lyrae, Red Giant Branch, Red Clump, Blue Loop and Asymptotic Giant Branch. The age distribution of the stars in each of the evolutionary phases can be seen in Fig. 2.3.

- Young 1 are very young main sequence stars aged below 50 Myr.
- Young 2 are young main sequence stars aged between 50 to 400 Myr.
- Young 3 are main sequence stars of mixed ages up to 1-2 Gyr.
- RR Lyrae are low-mass pulsating stars in their He-burning phase. Their pulsations have periods between 0.2 and 0.9 days and light curve amplitudes between 0.2 and 1.6 magnitude in the blue photometric band (Salaris & Cassisi 2005).
- The Red Giant Branch consists of stars who have finished their main-sequence life, burning of materials in the core have stopped and the stars become redder and bigger.
- The Clump of Red Giants (Red Clumps, RC) are the bright clump in the Red Giant Branch. These are low-mas stars which are in their He-burning phase. However, they burn Helium at a lower effective temperature than other stars which makes them appear more red (Girardi 2016).
- The Blue Loop (BL) refer to the loop made by blue stars with intermediate mass in an HR-diagram. The loop is created when the stars which have more mass burn Helium at a higher effective temperature and therefore are more blue. This takes

them further away from the RGB but they do a loop back (Salaris & Cassisi 2005; Karttunen et al. 2017).

- The Asymptotic Giant Branch (AGB) includes stars which have entered the phase of Helium burning in a shell around their core. Their effective temperature decreases and they become more luminous. They are quite similar to the stars in the RGB (Karttunen et al. 2017).

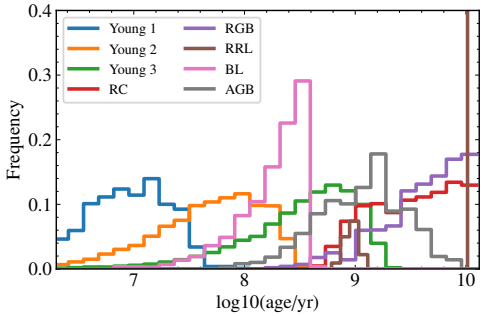

Figure 2.3: The age distribution of the stars in each of the evolutionary phases. Credit: Gaia Collaboration et al., A&A, 2021, 649, A7, reproduced with permission © ESO.

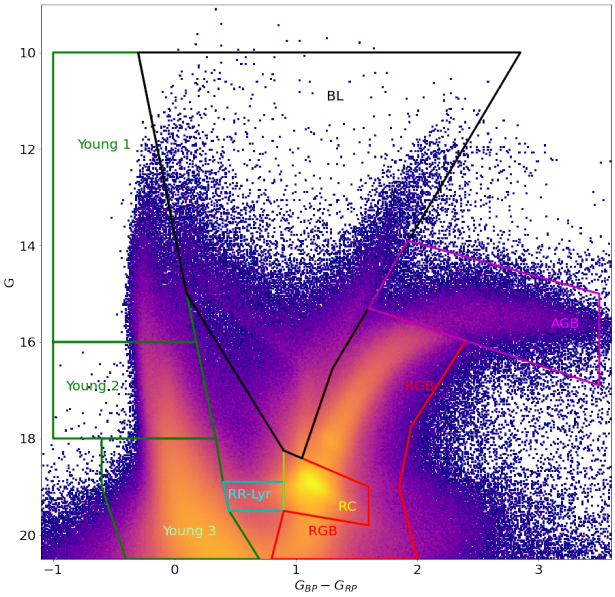

Figure 2.4: The Colour-Magnitude-Diagram of the data, the stars in the LMC. The eight sub samples are shown with the lines in different colours.

Table 2.1 shows the number of objects in each of these sub samples.

Total number of objects in LMC	12263084
Young 1 (Y1)	23900
Young 2 (Y2)	234016
Young 3 (Y3)	3599835
RR Lyrae (RRL)	226134
Red Clump (RC)	3761480
Red Giant Branch (RGB)	2682921
Blue Loop (BL)	264604
Asymptotic Giant Branch (AGB)	34095

Table 2.1: Number of objects in each of the evolutionary phases of the LMC.

The data in each sub sample was divided into bins on the sky. Each sub sample was divided into a 40×40 grid of bins over the area $-8° < x < 8°$, $-8° < y < 8°$, making the dimension of the bins 0.4 ° by 0.4 °. Objects within the same bin were put together and treated as a single data point. The binning is done in order to work with a smaller amount of data, to make it more efficient to analyse the different properties of the objects in each sample. This allows us to plot the proper motion of the objects in each sample in both the x-direction and y-direction. It also allows us to investigate the difference in proper motion of the various populations.

2.2 Model

To understand and analyse our data we need to fit them to a model. We use the model from Gaia Collaboration et al. (2021) which assumes that the LMC is a flat disk with unknown bulk velocity, inclination, orientation and internal velocities. We further need to chose a centre of rotation and a model for the internal velocities.

2.2.1 The model with three parameters

We start with the models for internal velocities from Gaia Collaboration et al. (2021),

$$\begin{aligned} v_\phi(R) &= \frac{v_0}{(1 + (r_0/R)^\alpha)^{(1/\alpha)}} \\ v_R(R) &= 0. \end{aligned} \tag{2.2}$$

It includes terms for the rotational velocity and the radial velocity as a function of radius divided by the distance to the LMC, R. The model assumes a centre at $(78.76°, -69.19°)$ of the The radial velocity is assumed to be zero for the entire LMC and the model for the rotational velocity depends on three parameters, v_0, r_0, α. The value of α determines the

smoothness of the curve. If the value of α is high, the curve has a sharp cut off while if it is a low value the curve will be smooth, see Fig. 2.5, where we also showed the dependence of r_0 and v_0. The parameter r_0 is also scaled with the distance to the galaxy and is the radius at where the rotational velocity curve flattens out, the breaking point. The parameter v_0 is the initial velocity and is given in mas/yr.

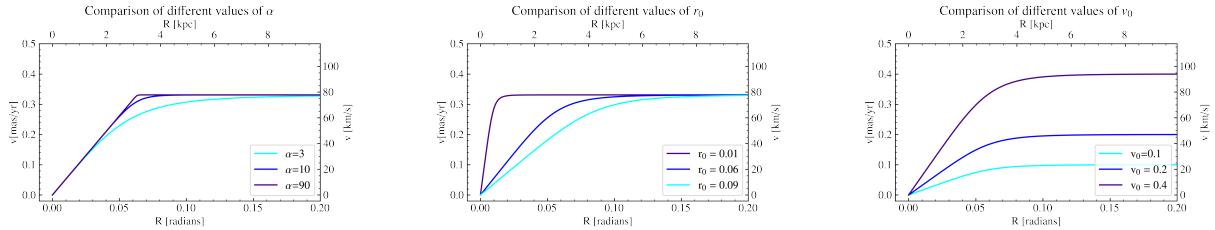

Figure 2.5: Curves with different values of α, r_0 and v_0 to demonstrate how they affect the shape of the curve. In the plot to the left we can see how the value of α affects the sharpness of the curve. In the plot in the middle the value of r_0 is changed to show how the curve is affected. The right-most plot shows the affect of v_0 on the curve.

The values of the parameters of the model were determined by minimising the difference between the observed proper motions and those predicted by the models, taking into account the observational uncertainties. This means that we minimise a chi-square-like statistic (for details see sec 5 of Gaia Collaboration et al. 2021). The parameters returned were μ_x, μ_y, inclination (i), orientation(ω), v_o, r_0, α.

This was done for each of the evolutionary phases. We also found the parameters when we masked the data to remove the objects in the inner part of the LMC, specifically a radius of 2°. This will produce parameters different to those determined using the unmasked data. Since the inclination and orientation will be different, the rotation curve will also differ from the one derived using unmasked data. The inner part of the LMC was removed in order to remove the bins where orbits and velocities can be most disturbed by the bar.

2.2.2 The model with four parameters

A model for the internal rotational velocity with an additional parameter was also used. This model also had the centre fixed at $(78.76°, -69.19°)$. Therefore we refer to this as the model with four parameters. For the radial velocity the model is still 0.

$$\begin{aligned} v_\phi(R) &= \frac{v_0}{(1 + (r_0/R)^\alpha - (r_1/R)^{\alpha/2})^{(1/\alpha)}} \\ v_R(R) &= 0. \end{aligned} \tag{2.3}$$

The parameters μ_x, μ_y, i, ω, v_o, r_0, r_1, α were determined in the same way as described above. The parameter r_1 is the distance at where the rotation curve starts to decrease.

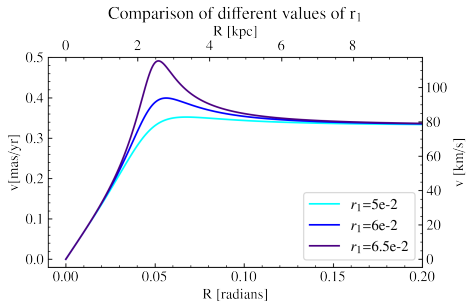

Figure 2.6: The model with 4 parameters using different values of r_1.

The model with three parameters does not have the flexibility to decrease at outer radii and this model allowed us to investigate whether this is important. Fig. 2.6 shows how the model depends on the parameter r_1.

2.2.3 The model with non-fixed centre

The model with three parameters, in eqn 2.2, was used to determine the parameters again but now, we allowed the rotational centre to be a free parameter. The parameters determined were α_0, δ_0, μ_x, μ_y, i, ω, v_o, r_0, r_1, α. Where α_0, δ_0 is the rotational centre. The model was used to determine the rotational centres for each of the eight sub samples.

The three different models were compared to each other in order to determine which best fit the data. The values for α_0, δ_0 derived using the free centre model were saved for each of the evolutionary phases. These were then plotted to compare the rotational centres for each of the evolutionary phases.

Chapter 3

Results

3.1 Proper Motion of the LMC

The evolutionary phases Young 3 and RGB are two of the phases with the largest number of stars and they have very different ages. The proper motion of these two evolutionary phases are shown in Fig. 3.1 and 3.2 respectively. There is a gradient across the disc for the proper motion in both direction for Young 3 and RGB which is typical for a rotating galaxy. We can also see disturbances near the centre due to the bar, especially in the plot showing the proper motion in the y-direction. These disturbances are located at approximately (2,0) to(-2,0) for both the Young 3 and RGB sub samples. The colour scheme represents the proper motion in units of mas/yr. Each colour pixel is one bin which contains many objects. The value shown is the median proper motion of the objects within the bin.

The difference in proper motion between stars in the two evolutionary phases Young 3 and RGB are presented in Fig. 3.3. In the plot for μ_x we can see two clear spots where there is a bigger difference between the two phases proper motion in the x-direction. This indicates that the stars in the sub sample Young 3 rotate faster than the stars in the sub sample RGB. In the plot for μ_y there is one clear spot where there is a bigger difference. We can also see traces of a spiral.

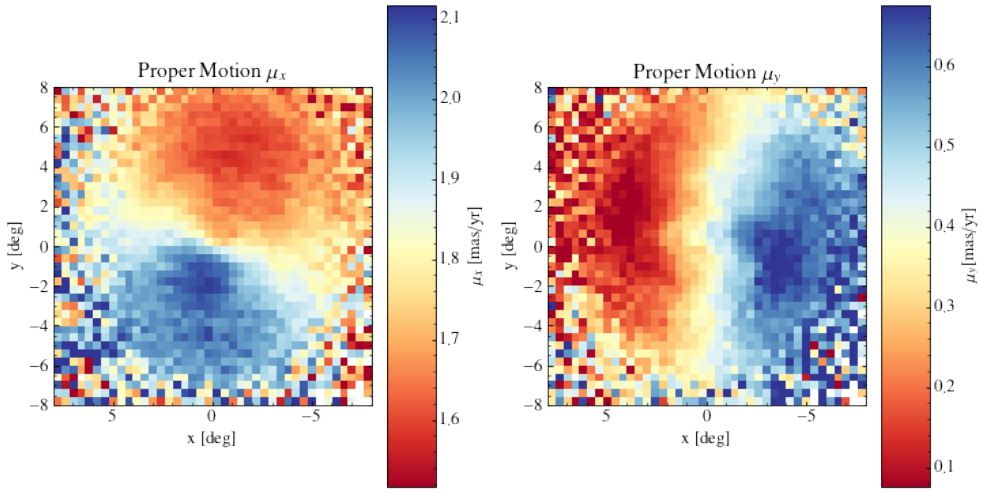

Figure 3.1: Proper motion of the Young 3 population.

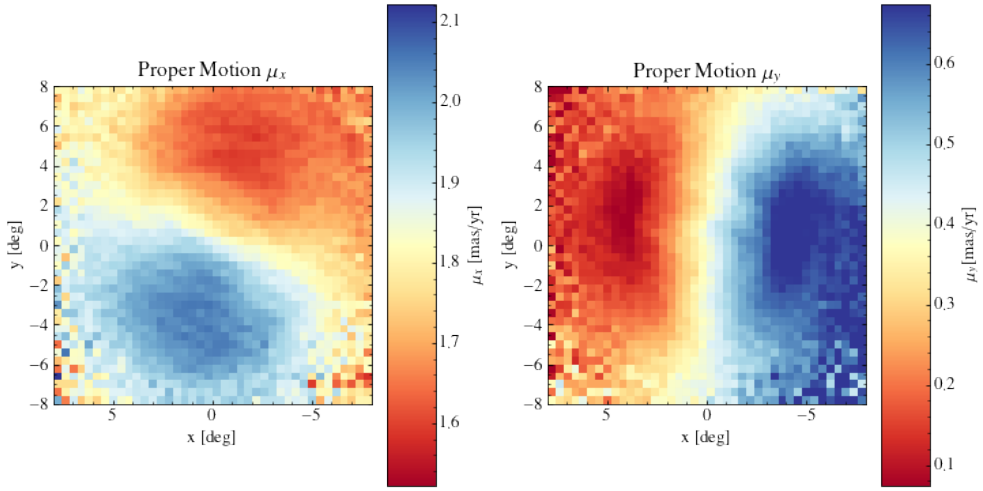

Figure 3.2: Proper motion of the RGB population.

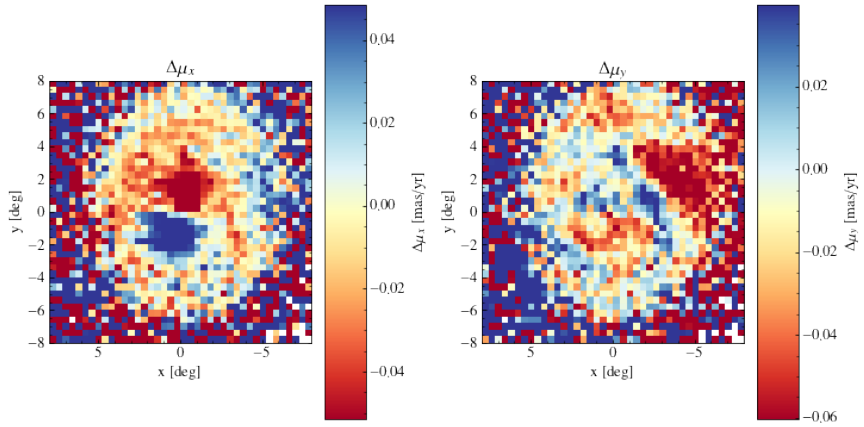

Figure 3.3: The difference in proper motion between Young 3 and RGB. These two populations are two of the biggest of the eight considered. This is why they were chosen for this comparison.

The plots of the proper motion for each of the other evolutionary phases can be seen in appendix 1.

3.2 Model with three parameters

The values for the parameters determined with the model with three parameters are presented in table 3.1.

Age Group	μ_x [mas/yr]	μ_y [mas/yr]	i [deg]	ω [deg]	v_0 [mas/yr]	r_0 [rad]	α
All stars	1.864	0.385	33.706	307.269	0.331	0.059	4.410
Young 1	1.871	0.350	41.195	295.047	0.573	0.029	0.877
Young 2	1.874	0.351	37.744	288.944	0.550	0.025	0.824
Young 3	1.866	0.370	34.182	298.455	0.393	0.043	1.546
RRL	1.865	0.394	34.479	304.303	0.303	0.066	6.363
RC	1.861	0.393	34.397	312.018	0.329	0.067	6.165
RGB	1.869	0.387	34.745	310.665	0.331	0.063	4.612
BL	1.867	0.379	32.875	298.840	0.367	0.042	2.338
AGB	1.906	0.367	35.606	306.703	0.379	0.058	2.965

Table 3.1: Parameters of the evolutionary phases of the LMC determined using the model with three parameters.

In Fig. 3.4 we compare the model to the data in both the rotational and radial velocities for Young 3. The same plots for RGB are shown in figure 3.5. In these cases, the coordinate system used is an internal coordinate system in the LMC as if seen face on when the inclination would be 0°. The values of the parameters used for this model for each of the evolutionary populations are presented in Tab. 3.1. The values of the parameters

for the different sub samples are quite close for the majority of the parameters. Therefore three decimal numbers were used in order to show the differences. Note that the number of significant digits were not chosen based on the uncertainties of the values and can therefore be too many but they were chosen so that we can see a difference between them. In Fig: 3.4 in the plot for the rotational velocity we can see faint structures of spiral arms. This can be seen in the plot for the rotational velocity for RGB in Fig. 3.5 as well. The plots of the radial velocities do not have the model value subtracted.

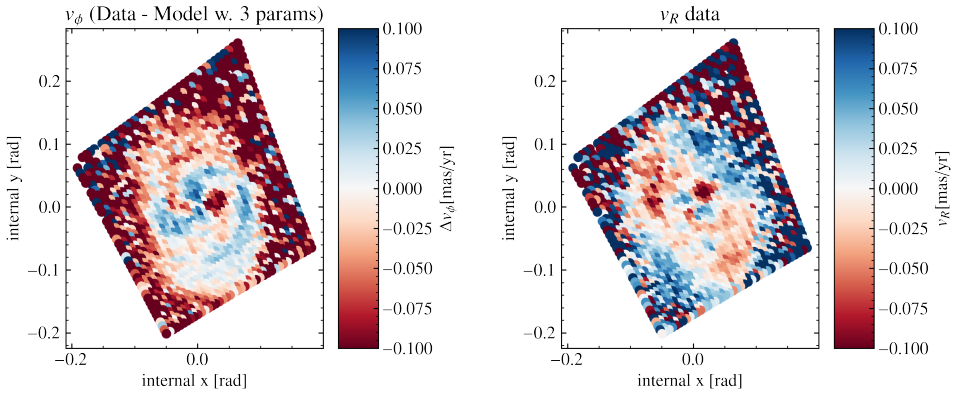

Figure 3.4: The plots compare the model with 3 parameters to the data for the radial and rotational velocities for the sub sample Young 3.

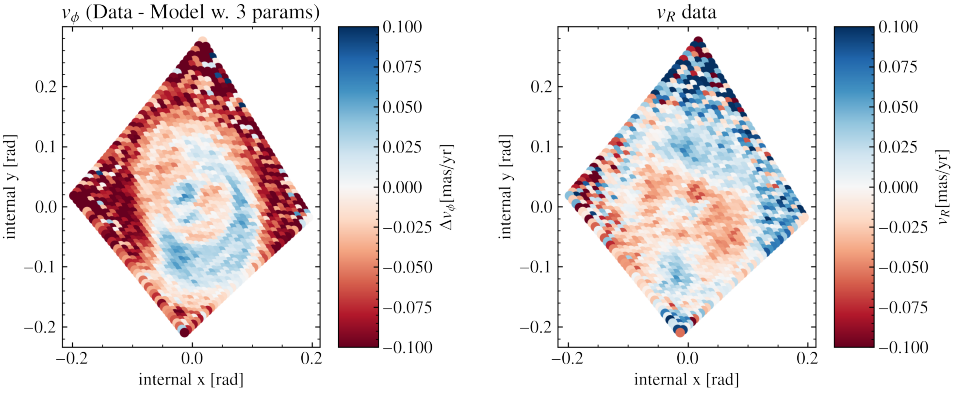

Figure 3.5: The plots compare the model with 3 parameters to the data for the radial and rotational velocities for the sub sample RGB.

The equivalent plots for Figs. 3.6 & 3.7 for all evolutionary phases are shown in appendix 1.

The model with three parameters are plotted with masked and unmasked data for Young 3 in Fig. 3.6 and for RGB in Fig. 3.7. The x-axis is both in radians and kpc and 1 rad = 49.59 kpc. The y-axis is in both mas/yr and km/s, 1 mas/yr = 235 km/s. We see that the difference between the rotation curves in the plot is very small but slightly bigger

for RGB. The decision was made to not mask the data for the analysis. Regardless of the data being masked or not, the biggest difference between the data and the model is at the outer parts of the galaxy. The model shows a higher velocity for the majority of the curve but the difference is much bigger after the curve have flatten out, especially for the RGB. The velocity of the data starts to decrease again but the model is not complex enough to do this. The values of the parameters determined with the model with 3 parameters with masked data are presented in table 3.2.

Age Group	μ_x [mas/yr]	μ_y [mas/yr]	i [deg]	ω [deg]	v_0 [mas/yr]	r_0 [rad]	α
Young 1	1.864	0.362	36.674	302.794	0.482	0.022	0.958
Young 2	1.860	0.353	32.959	299.076	0.375	0.045	2.693
Young 3	1.859	0.367	32.084	308.073	0.327	0.061	5.768
RRL	1.861	0.393	33.550	307.811	0.294	0.072	50.000
RC	1.855	0.390	34.366	314.433	0.322	0.072	16.012
RGB	1.859	0.383	34.609	314.074	0.320	0.071	14.424
BL	1.856	0.375	31.350	309.387	0.337	0.058	6.458
AGB	1.898	0.364	34.749	309.715	0.358	0.068	7.245

Table 3.2: Parameters of the evolutionary phases of the LMC determined using the model with three parameters using masked data.

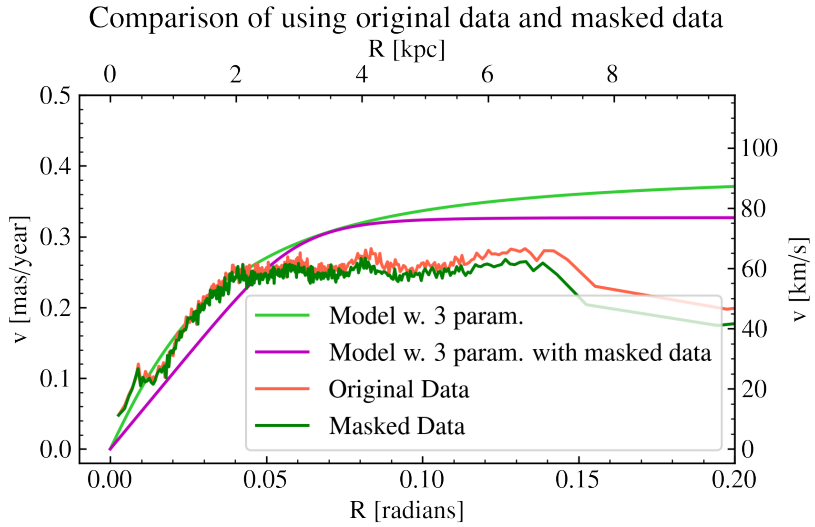

Figure 3.6: The model with three parameters used with the masked and unmasked data for Y3

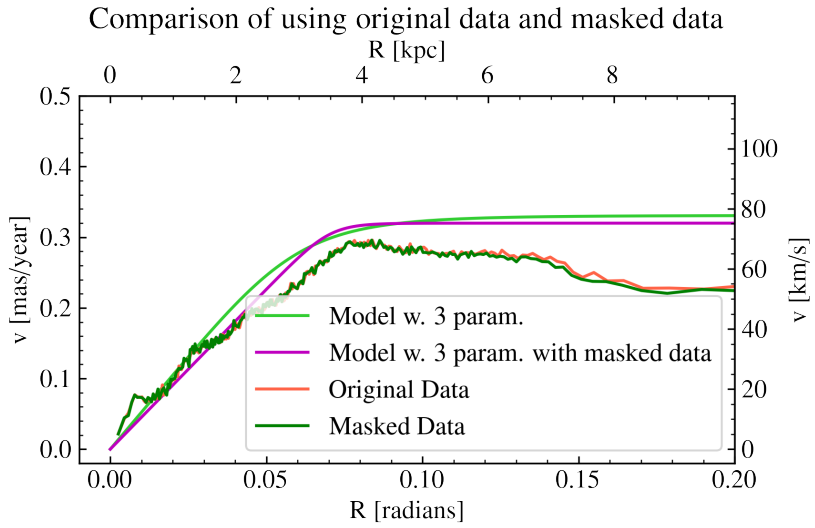

Figure 3.7: The model with three parameters used with the masked and unmasked data. for RGB

3.3 Model with 4 parameters

The model with four parameters was introduced in hope of solving the problem of the velocity decreasing for the data and not the model. The values of the parameters determined with the model with four parameters can be seen in table 3.3.

Age Group	μ_x [mas/yr]	μ_y [mas/yr]	i [deg]	ω [deg]	v_0 [mas/yr]	r_0 [rad]	r_1 [rad]	α
Young 1	1.871	0.350	41.187	295.043	0.234	0.029	0.035	0.411
Young 2	1.874	0.351	37.748	288.916	0.198	0.025	0.035	0.378
Young 3	1.866	0.370	34.233	298.446	0.083	0.042	0.182	0.442
RRL	1.865	0.394	34.438	304.333	0.297	0.066	0.048	4.281
RC	1.861	0.393	34.395	312.017	0.328	0.067	0.032	5.655
RGB	1.869	0.387	34.745	310.666	0.331	0.063	0.000	4.612
BL	1.867	0.378	33.929	297.778	0.366	0.044	0.002	2.557
AGB	1.906	0.367	35.619	306.629	0.094	0.057	0.216	0.602

Table 3.3: Parameters of the evolutionary phases of the LMC determined using the model with four parameters.

The comparison of the two models are plotted for the Young 3 in Fig. 3.8 and for the RGB in Fig. 3.9. The difference between them are close to non-existent. Since the model with four parameters does not fit the data better than the model with 3 parameters, the decision was made to continue with the model with three parameters.

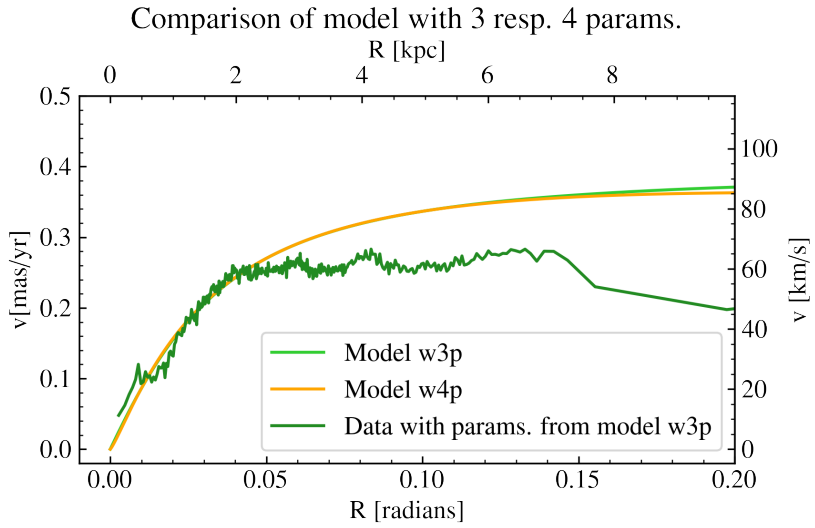

Figure 3.8: Model with 3 parameters (w3p) compared to the model with 4 parameters (w4p) for Young 3. The data plotted using the parameters of the model with 3 parameters is indistinguishable from the data plotted using the parameters of the model with 4 parameters, so we only show one of these curves.

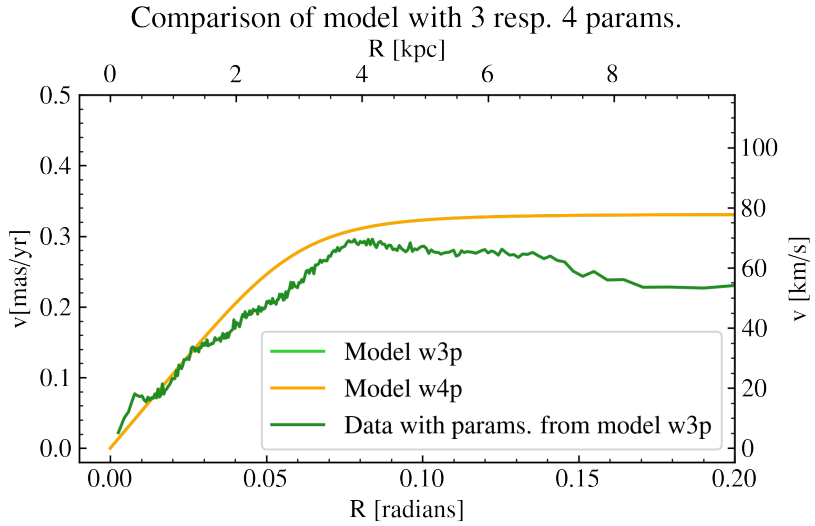

Figure 3.9: Model with 3 parameters (w3p) compared to the model with 4 parameters (w4p) for Young RGB. The data plotted using the parameters of the model with 3 parameters is indistinguishable from the data plotted using the parameters of the model with 4 parameters, so we only show one of these curves.

3.4 Model with a non-fixed centre

Finally, we leave the centre as a free parameter. In section 3.2 we showed that the masking of the inner 2°does not provide enough improvement of the fit to the data to keep masking the data. In section 3.3 we showed that the model with 4 parameters did not provide a significant improvement and therefore the non-fixed centre was applied on to the model with three parameters and not the model with four parameters. We therefore refer to the model with a non-fixed centre as "the model with a free centre". The model with three parameter with a fixed centre is referred to as "model with three parameters" or "model with fixed centre". The values of the parameters determined with this model is presented in table 3.4.

Age Group	α_0 [deg]	δ_0 [deg]	μ_x [mas/yr]	μ_y [mas/yr]	i [deg]	ω [deg]	v_0 [mas/yr]	r_0 [rad]	α
Young 1	81.181	-69.798	1.873	0.350	39.114	292.843	0.455	0.033	1.419
Young 2	81.106	-69.606	1.858	0.341	35.609	290.550	0.391	0.030	1.714
Young 3	80.817	-69.521	1.854	0.346	32.953	306.237	0.324	0.043	2.882
RRL	81.477	-69.522	1.851	0.403	33.231	305.342	0.290	0.065	10.177
RC	81.107	-69.398	1.846	0.381	34.066	312.633	0.312	0.066	17.321
RGB	81.191	-69.356	1.847	0.377	34.093	312.729	0.312	0.064	10.191
BL	81.054	-69.315	1.838	0.367	31.937	301.651	0.317	0.041	4.643
AGB	81.085	-69.287	1.889	0.354	33.918	308.970	0.355	0.057	4.267

Table 3.4: Parameters of the evolutionary phases of the LMC determined using the model with three parameters and a free centre.

The comparison of the rotation curves using the model with three parameters and the model with a free centre is shown in Fig. 3.10 for Young 3 and Fig. 3.11 for RGB. The data is based on the parameters determined using the respective model. We can see that the model with a free centre is closer to the data than the model with a fixed centre is. In the outer parts of the galaxy the model with a non-fixed centre is still at too high velocities compared to the data. The fit is better than the previous fits until approximately 6 kpc.

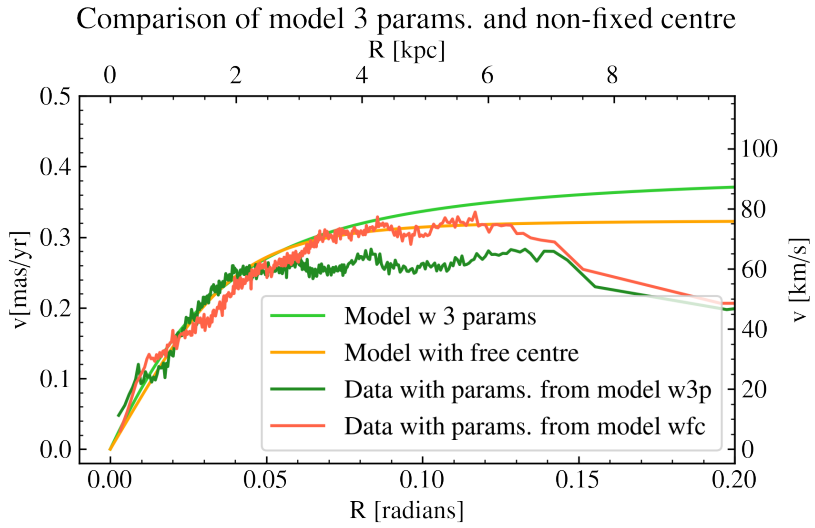

Figure 3.10: Comparison of the rotation curve between the model with 3 parameters and the model with a free centre for Young 3.

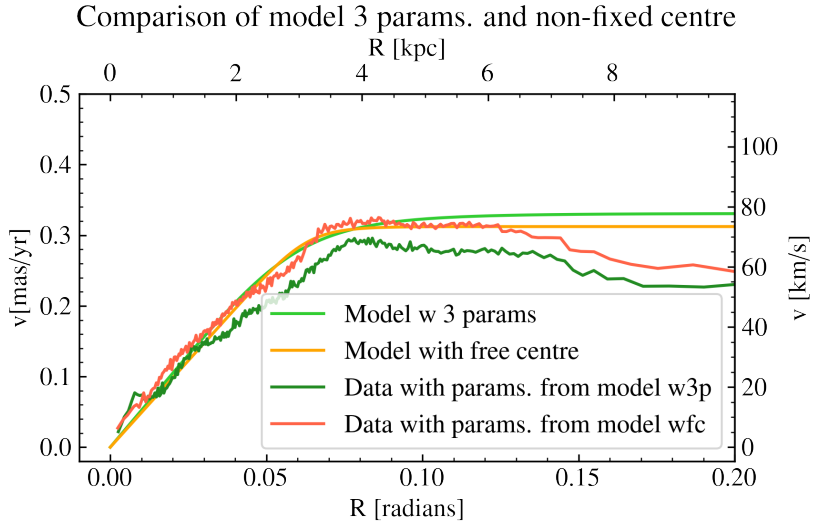

Figure 3.11: Comparison of the rotation curve between the model with 3 parameters and the model with a free centre for RGB

Figs. 3.12 and 3.13 show the difference in two dimensions of the data and the model with a free centre for the populations Young 3 and RGB respectively. The two plots of the rotational velocities show structures of spiral arms. We can also see the uttermost part of the galaxy differs more, which we also can see in Figs. 3.10 & 3.11.

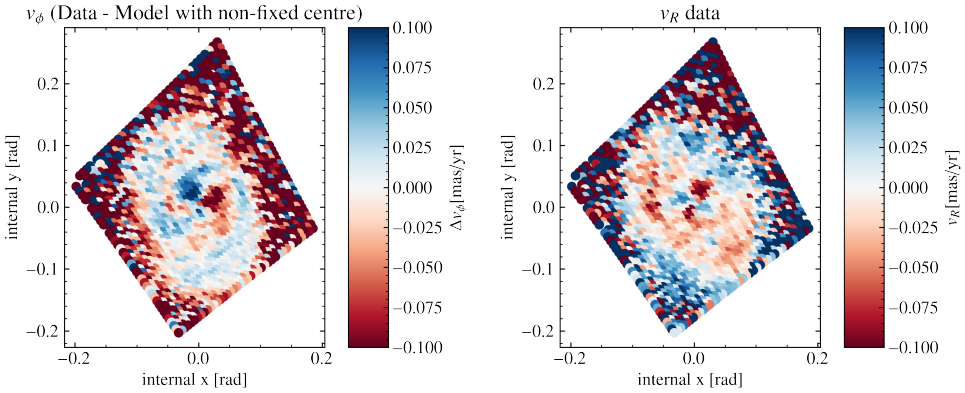

Figure 3.12: Comparison between the data and the model with a non-fixed centre for the rotational velocity and the radial velocity for the evolutionary phase Young 3.

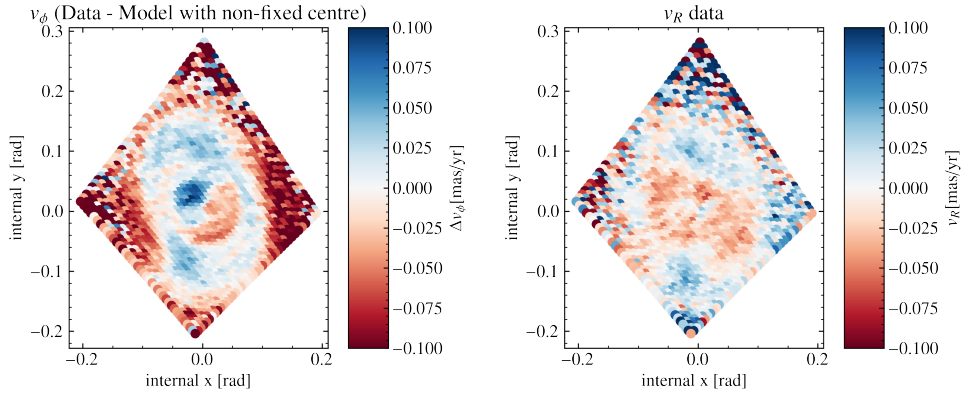

Figure 3.13: Comparison between the data and the model with a non-fixed centre for the rotational velocity and the radial velocity for the evolutionary phase RGB.

The model with a non-fixed centre for all the stellar populations are shown in Fig. 3.14. The data was not included in this plot for any of the populations. The model is used to compare the difference between the rotation curves for the different populations. Note that the models are not perfect and the figure is only shown for demonstration.

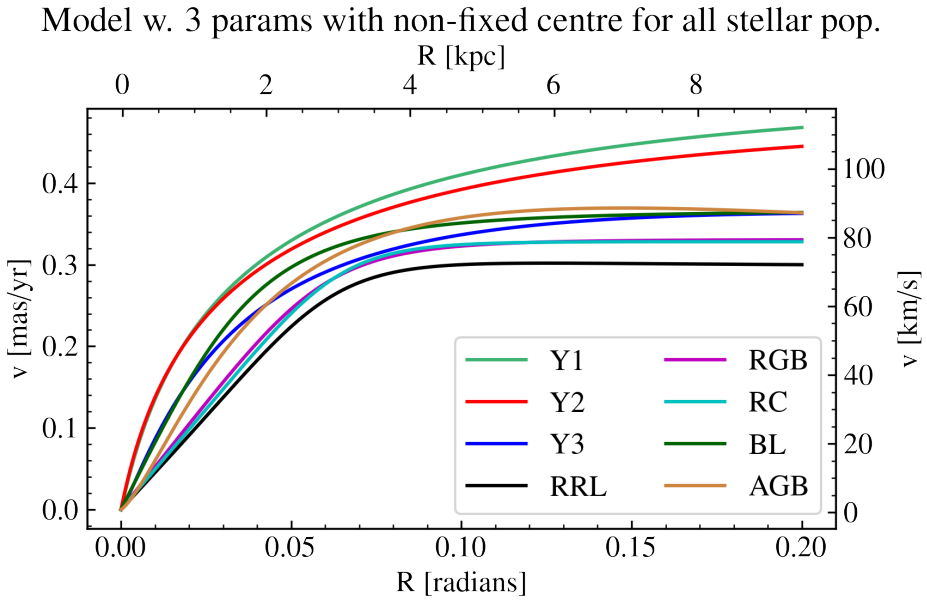

Figure 3.14: The model with 3 parameters with a non-fixed centre plotted for every stellar population.

Fig. 3.15 shows the density of stars in the central parts of the LMC. The faint spiral structure can be seen together with the bar at approximately $(\alpha, \delta) = (-70°, 75°)$. The red and blue square show the parts which are zoomed in in Figs. 3.16 & 3.17 respectively.

Fig. 3.16 are the density of stars within the red square in Fig. 3.15. The rotational centres for each of the evolutionary phases observed in this work are located within this square. The initial guess (IG) is the photometric centre found by van der Marel (2001) using the Hubble Space Telescope, (81.28°, -69.78°).

Fig. 3.17 shows the density of stars within the blue rectangle in Fig. 3.15. The reason for this being less zoomed in is because the centres found in other articles are further away. The centres of the population observed in this these are too close together in order to be clearly visible in Fig. 3.17. Therefore they are presented in another Fig. than the previously found centres.

Wan et al. (2020) found the rotational centre of the RGB population to be (81.23, -69.00) and the centre of the Young population to be at (80.98, -69.69). Note that these populations were not chosen in the exact same way as the population used in this article. Kim et al. (1998) found the centre for the HI gas disc to be (79,40, -69.03) while Luks & Rohlfs (1992) found it to be (78.13, -69.00). van der Marel & Kallivayalil (2014) found a rotational centre of the LMC using the Hubble Space Telescope (HST) at (78.76, -69.19). Gaia Collaboration et al. (2021) derived a rotational centre of (81.01, -69.38). The rotational centres for each evolutionary phase I have determined are presented in table 3.5.

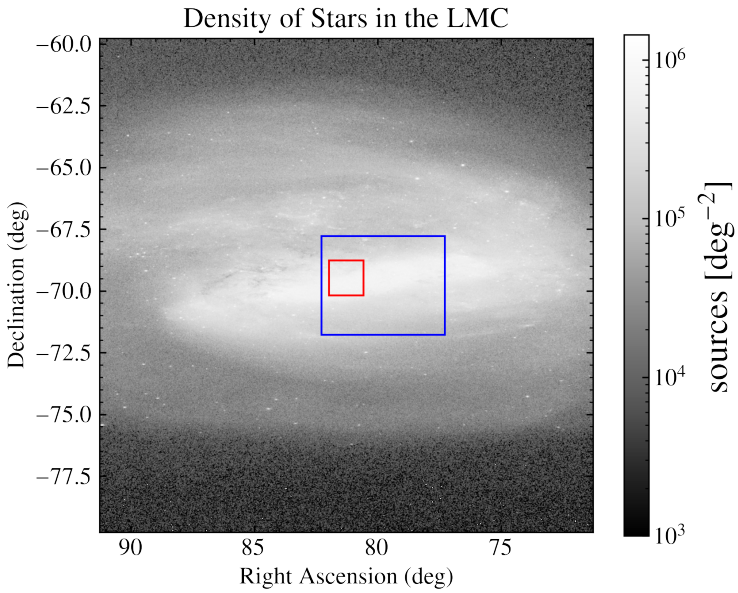

Figure 3.15: The sky density of stars of the LMC. The red square represents the part of the plot which is the zoomed in spot in figure 3.16. The blue square represents the part of the plot which is the zoomed in spot in Fig. 3.17.

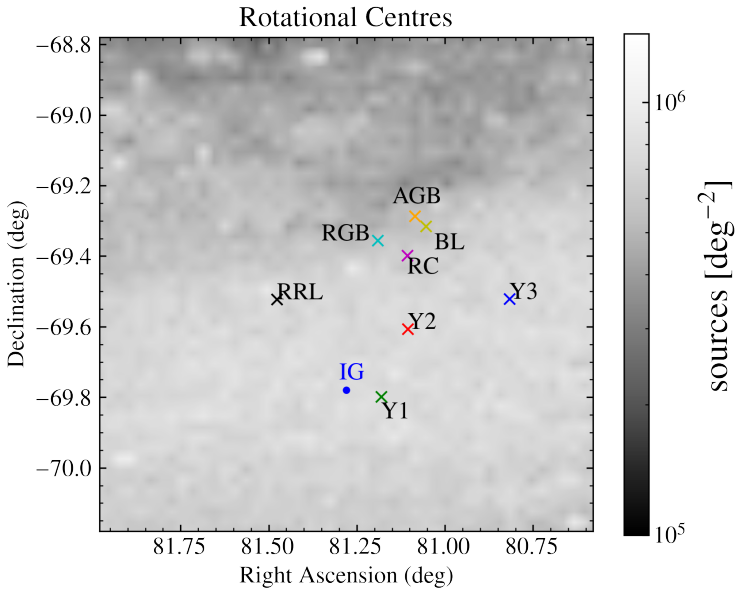

Figure 3.16: The rotational centres of the chosen stellar populations.

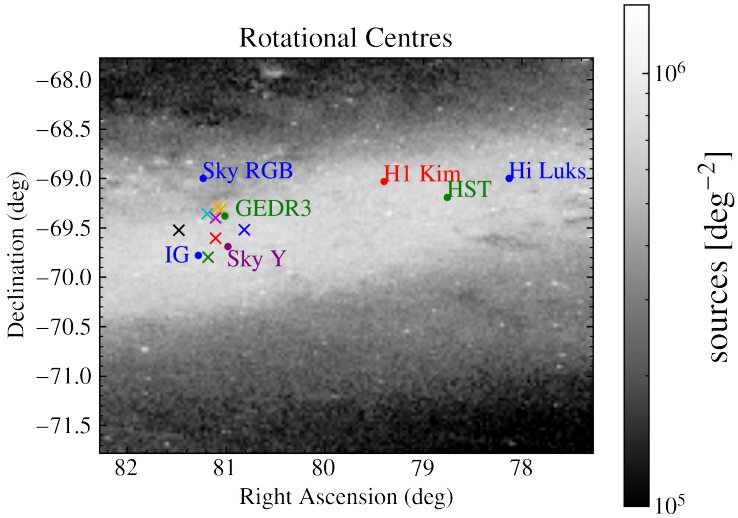

Figure 3.17: Rotational centres found in previous observations. The positions labelled Sky RGB and Sky Young are collected from Wan et al. (2020). The Initial guess is collected from van der Marel (2001) and HI is collected from van der Marel & Kallivayalil (2014).

Population	Right Ascension (α_0)	Declination (δ_0)
Young 1	81.181	-69.798
Young 2	81.106	-69.606
Young 3	80.817	-69.521
RRL	81.477	-69.522
RC	81.107	-69.398
RGB	81.191	-69.356
BL	81.054	-69.315
AGB.	81.085	-69.287

Table 3.5: Positions of the rotational centres for each of the stellar populations. These are plotted in Fig. 3.16.

Chapter 4

Conclusions

To summarise, in this thesis we have studied eight evolutionary phases in the Large Magellanic Cloud. The proper motion of the stars in each of the sub samples have been examined. Three models have been fitted to the data to determine a rotation curve for each of the populations. A model with the centre left as a free parameter was used to determine the rotational centres for each of the sub samples.

The centres determined in this thesis which are furthest apart are the centres for Y1 and AGB. The angle between them is 0.57° which corresponds to a projected distance of 0.49 kpc. The angle between the two centres, determined by Wan et al. (2020), Sky RGB and Sky Young is 0.73° which corresponds to a projected distance of 0.63 kpc. The centres determined by Kim et al. (1998), Luks & Rohlfs (1992) for HI gas and van der Marel & Kallivayalil (2014) using HST are further away, the centre derived derived with HST is 1.07 kpc from the centre we determined for AGB.

The reason for the determined centres being closer together than the centres determined by other authors could mean that the inner dynamics of the LMC has been less affected by the interactions than what previously have been thought. Kim et al. (1998) and Luks & Rohlfs (1992) determined centres using HI gas. This could mean that the gas has been more affected by the interactions than the stars have been. This could be supported by the fact that the Magellanic Bridge was produced by stripped gas only. However, if this was true we would expect to have seen a bigger difference between the rotation centres for the younger and older stellar populations.

For the centres derived in this thesis, the older populations have higher declination than the younger populations. This is also seen in the centres derived by Wan et al. (2020) where the centre for the RGB population is higher in declination than the centre for the Young population. This may imply that the younger populations have been affected differently by the interactions than the older populations. The younger populations are closer to the centre of the bar which could mean that the bar has affected the younger populations more so that they ended up closer to it than the older stars.

The stars within the Blue Loop are not behaving like the other younger populations. The rotational centre of the BL have higher declination. In the dividing of the stars into evolutionary phases, the edges for the BL are very close to the Red Giant Branch. Therefore

Red Giants, might contaminate the sub sample for the Blue Loop. The edge also cuts very close to the Red Clumps which are also older stars, and may also have contaminated the sample.

To better understand the interactions between the LMC and the SMC one could do simulations of the interactions. This could reveal more detail of how they have interacted and how the different stellar populations have been affected based on when the strongest interactions happened.

Future work may include a more careful calculation of the uncertainties of our derived values. We have followed the assumption made by Gaia Collaboration et al. (2021), who found that the systematic errors, the uncertainties of the models, are much greater than the statistical uncertainties, the uncertainties of the measured values by Gaia. By looking at the plots comparing the data to the fitted models, we can see that the models are poor fits to the data in many ways (though improved when we allow a non-fixed centre. The models are not used to derive specific values of the rotational velocities but to analyse how the rotational velocity behaves depending in radius.

Future work may also include careful analysis of the spiral arms of the LMC. They are not mapped with great detail. We can see structures of spiral arms and a structure of the bar. One could also include measured radial velocities to more accurately find the rotation curves of the stellar populations in order to determine the centres more carefully.

The rotational centre of the HI could also be analysed again. The observations which determined the centres referred to in this thesis were taken and analysed in 1992 and 1998. The instruments have been improved since then, as have analysis techniques and perhaps the centres would be found somewhere else.

Bibliography

Bagheri, G., Cioni, M. R. L., & Napiwotzki, R. 2013, A&A, 551, A78

Besla, G., Kallivayalil, N., Hernquist, L., et al. 2012, MNRAS, 421, 2109

Cautun, M., Benítez-Llambay, A., Deason, A. J., et al. 2020, MNRAS, 494, 4291

Erkal, D. 2019, in A Synoptic View of the Magellanic Clouds: VMC, Gaia and Beyond, 33

Gaia Collaboration, Luri, X., Chemin, L., et al. 2021, A&A, 649, A7

Gaia Collaboration, Prusti, T., de Bruijne, J. H. J., et al. 2016, A&A, 595, A1

Girardi, L. 2016, ARA&A, 54, 95

Harris, J. 2007, ApJ, 658, 345

Hindman, J. V., Kerr, F. J., & McGee, R. X. 1963, Australian Journal of Physics, 16, 570

Karttunen, H., Kröger, P., Oja, H., Poutanen, M., & Donner, K. J. 2017, Fundamental Astronomy

Kim, S., Staveley-Smith, L., Dopita, M. A., et al. 1998, ApJ, 503, 674

Luks, T. & Rohlfs, K. 1992, A&A, 263, 41

Pietrzyński, G., Graczyk, D., Gallenne, A., et al. 2019, Nature, 567, 200

Salaris, M. & Cassisi, S. 2005, Evolution of Stars and Stellar Populations (Wiley)

van der Marel, R. P. 2001, AJ, 122, 1827

van der Marel, R. P. & Kallivayalil, N. 2014, ApJ, 781, 121

Wan, Z., Guglielmo, M., Lewis, G. F., Mackey, D., & Ibata, R. A. 2020, MNRAS, 492, 782

Appendix A

This is an appendix

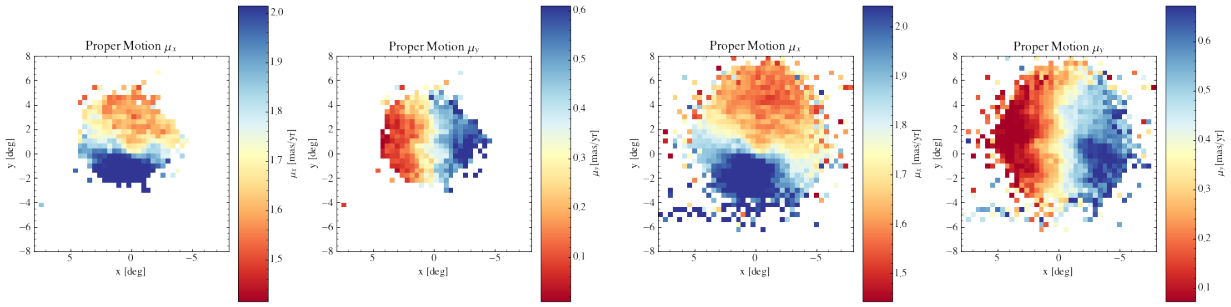

(a) Young 1 (b) Young 2

Figure A.1: Proper Motion of the Young 1 and Young 2 populations.

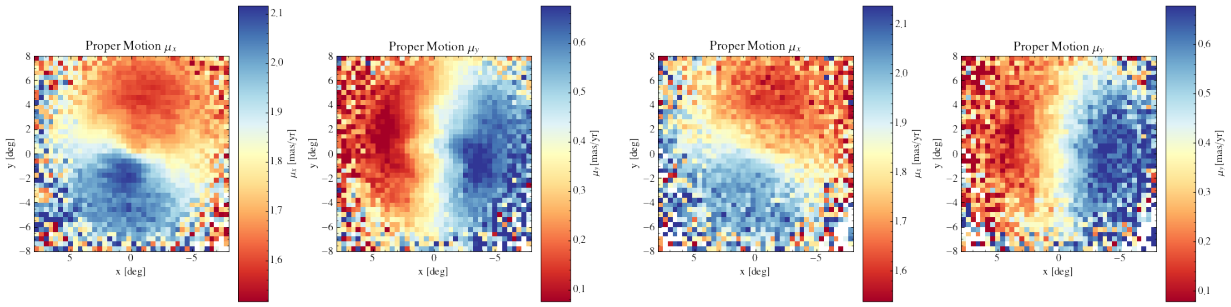

(a) Young 3 (b) RRL

Figure A.2: Proper Motion of the Young 3 and RRL populations.

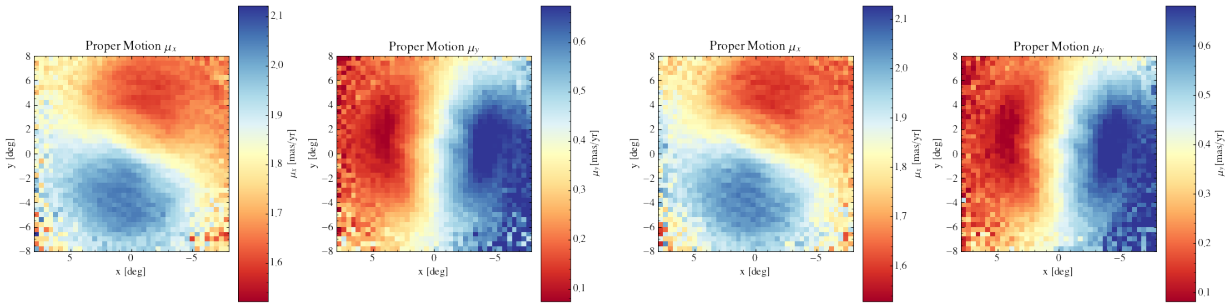

(a) RGB (b) RC

Figure A.3: Proper Motion of the RGB and RC populations.

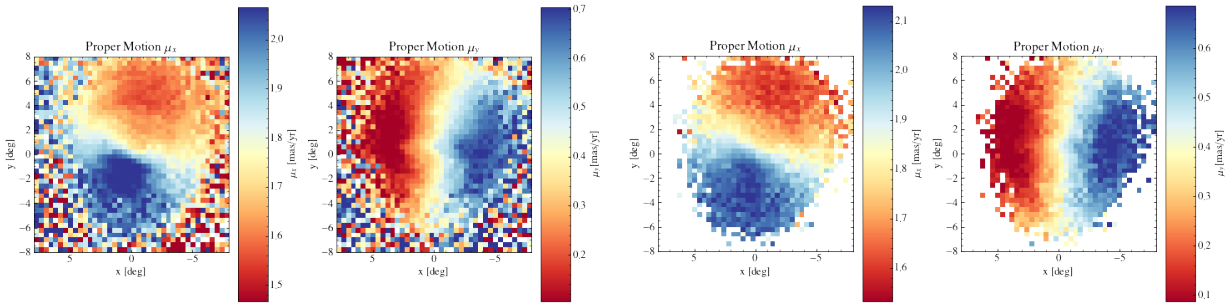

(a) BL (b) AGB

Figure A.4: Proper Motion of the BL and AGB populatoins.

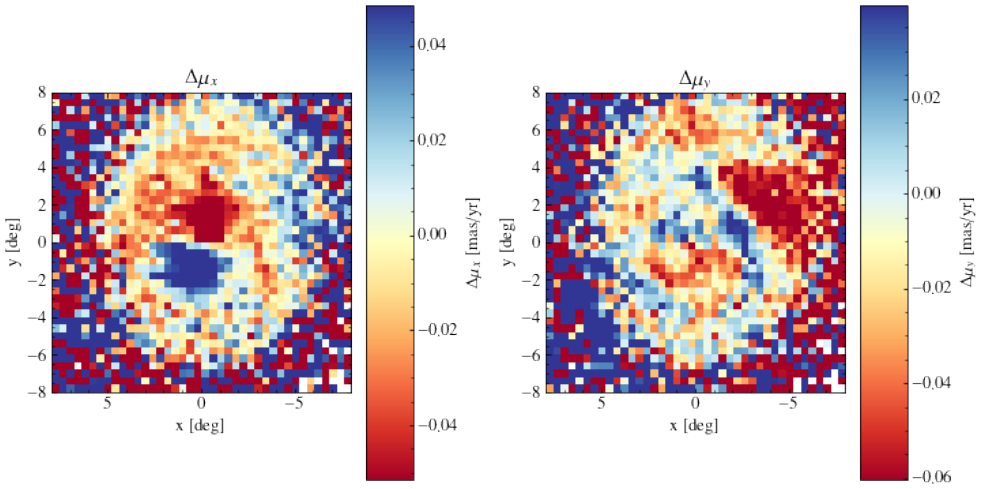

Figure A.5: The difference in proper motion between Young 3 and RGB. These two populations are two of the biggest of the eight populations. Due to that they were chosen to compare the proper motion between

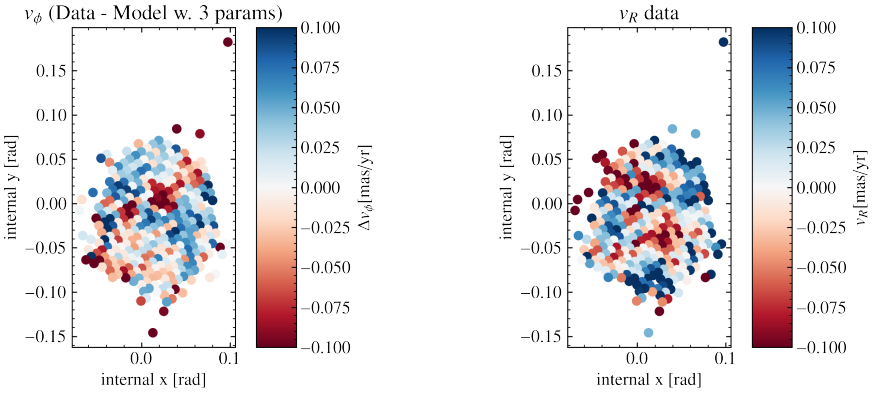

Figure A.6: Comparison between the model with 3 parameters and the data for radial velocity and rotational velocity for the evolutionary phase Young 1.

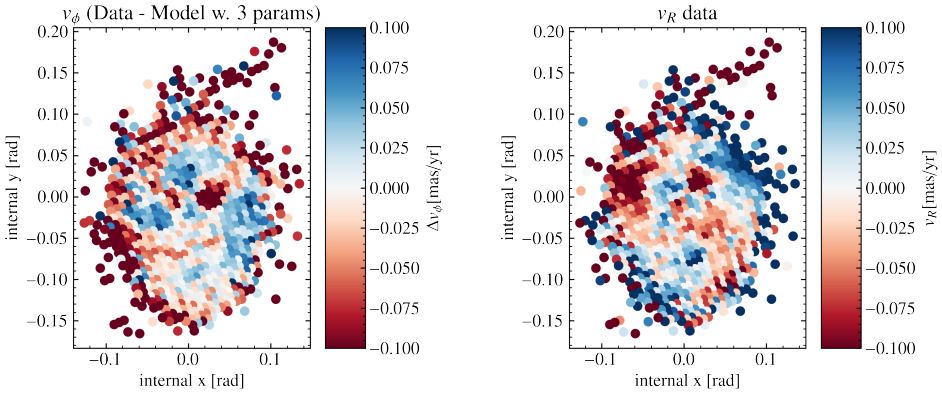

Figure A.7: Comparison between the model with 3 parameters and the data for radial velocity and rotational velocity for the evolutionary phase Young 2.

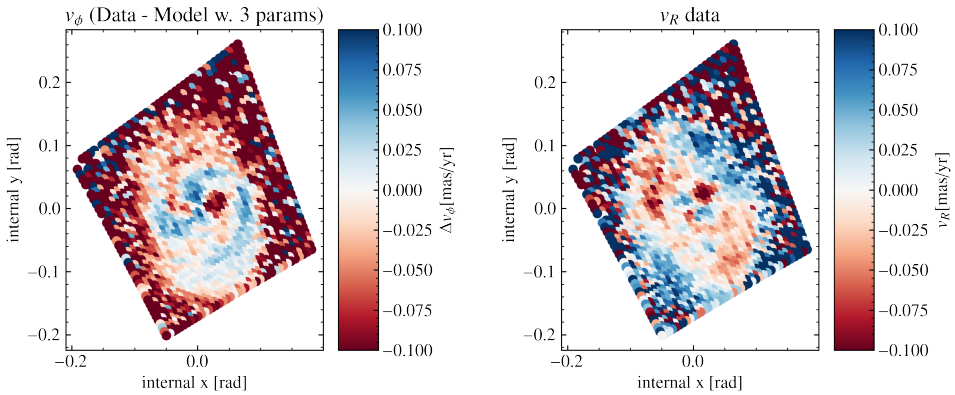

Figure A.8: Comparison between the model with 3 parameters and the data for radial velocity and rotational velocity for the evolutionary phase Young 3.

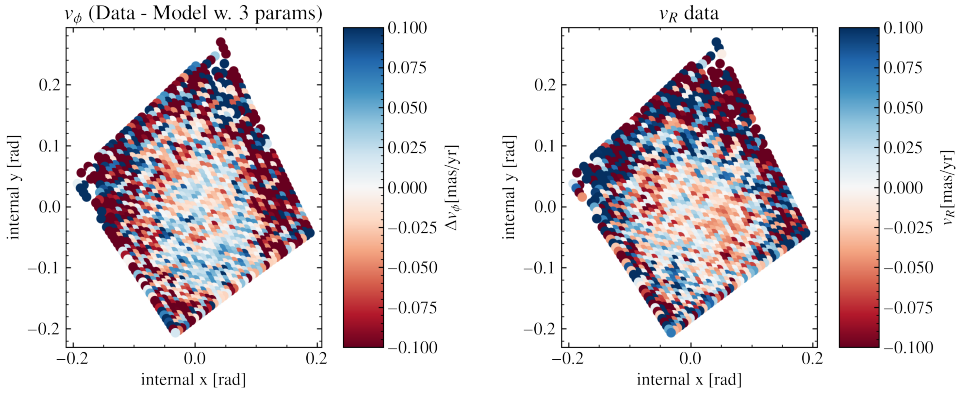

Figure A.9: Comparison between the model with 3 parameters and the data for radial velocity and rotational velocity for the evolutionary phase RRL.

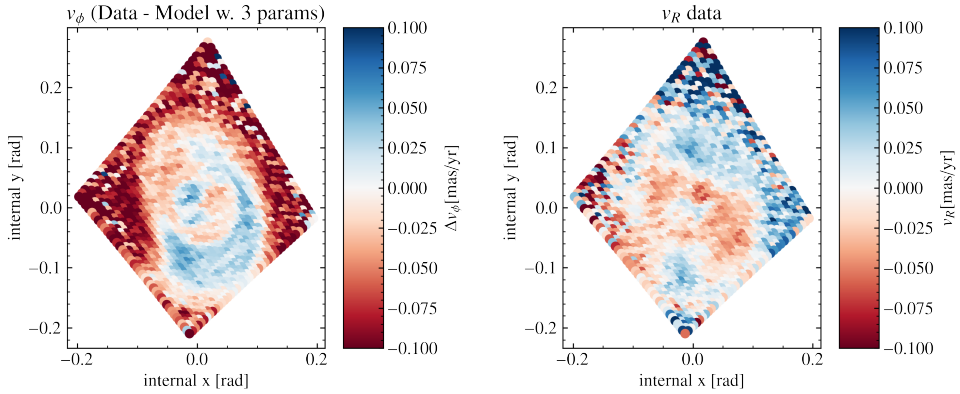

Figure A.10: Comparison between the model with 3 parameters and the data for radial velocity and rotational velocity for the evolutionary phase RGB.

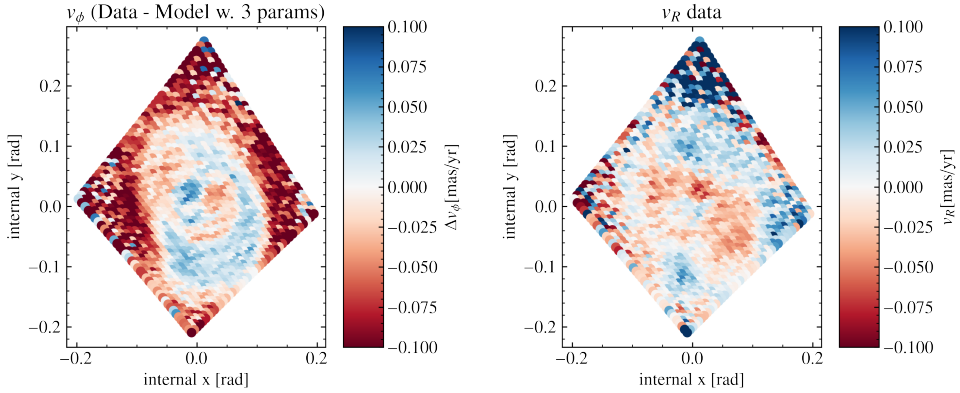

Figure A.11: Comparison between the model with 3 parameters and the data for radial velocity and rotational velocity for the evolutionary phase RC.

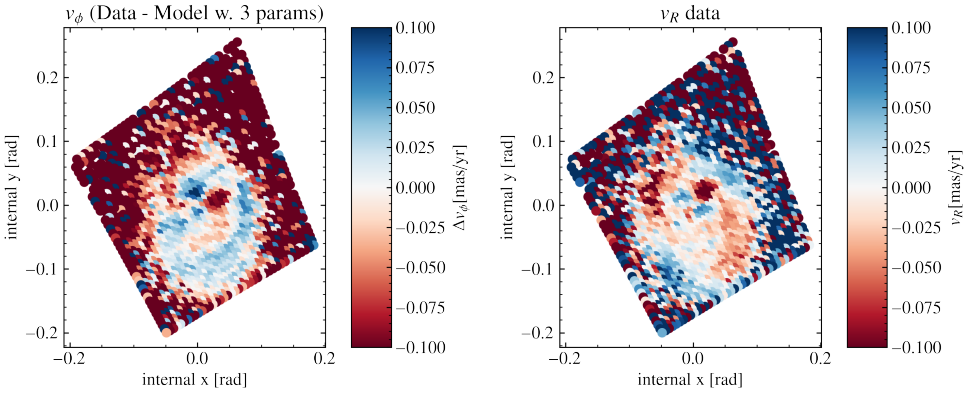

Figure A.12: Comparison between the model with 3 parameters and the data for radial velocity and rotational velocity for the evolutionary phase BL.

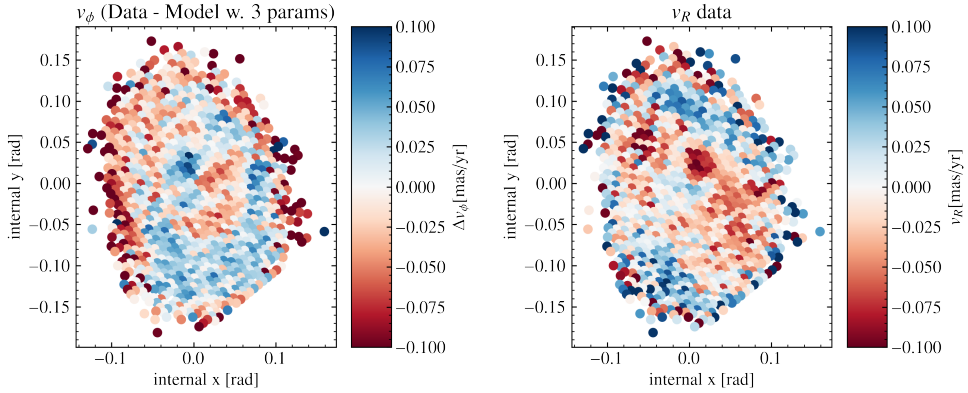

Figure A.13: Comparison between the model with 3 parameters and the data for radial velocity and rotational velocity for the evolutionary phase AGB.

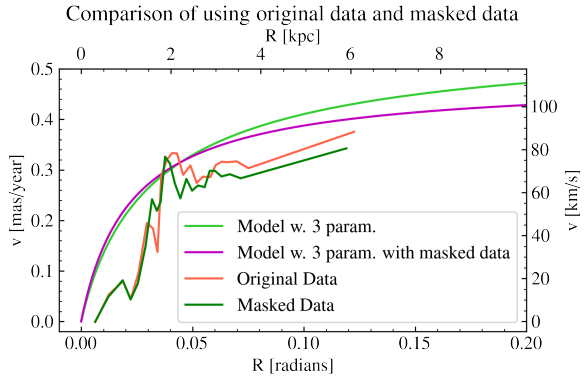

Figure A.14: The model with three parameters used with the masked and unmasked data for Y1

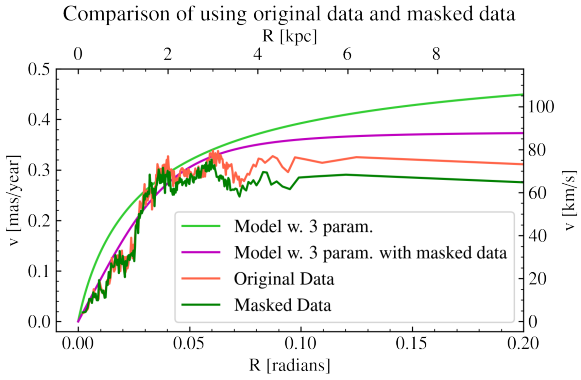

Figure A.15: The model with three parameters used with the masked and unmasked data for Y2

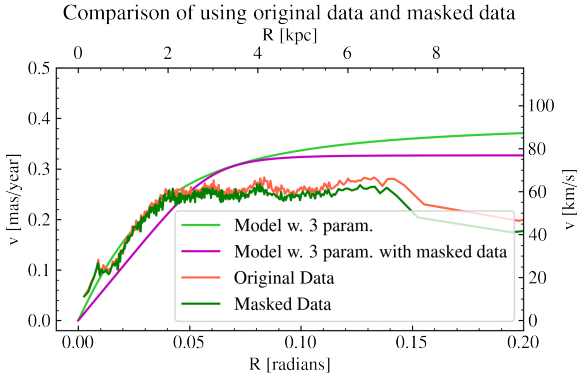

Figure A.16: The model with three parameters used with the masked and unmasked data for Y3

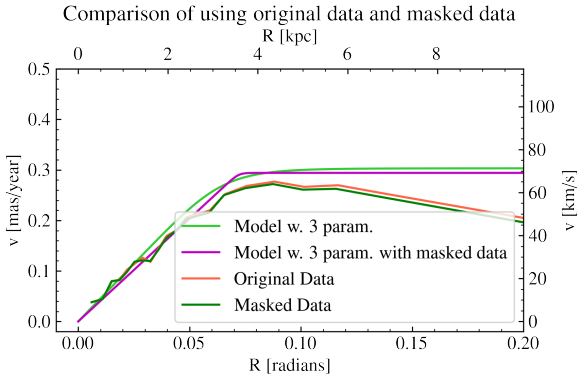

Figure A.17: The model with three parameters used with the masked and unmasked data for RRL

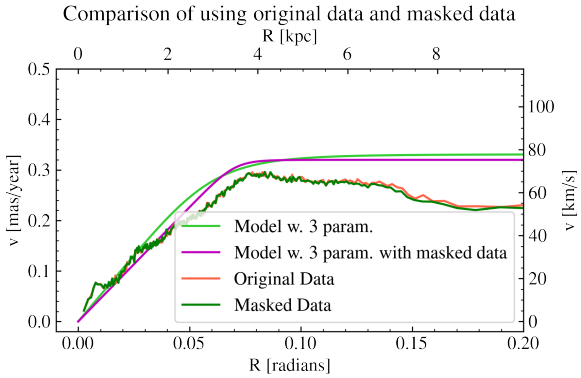

Figure A.18: The model with three parameters used with the masked and unmasked data for RGB

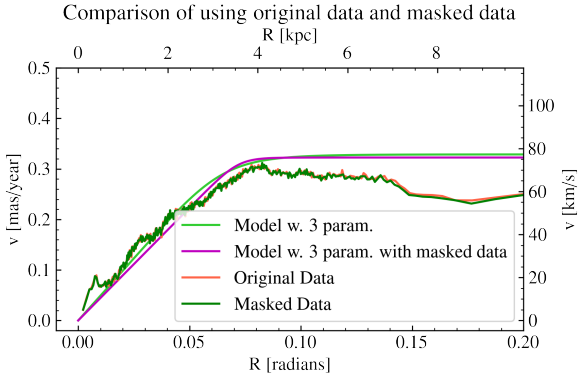

Figure A.19: The model with three parameters used with the masked and unmasked data for RC

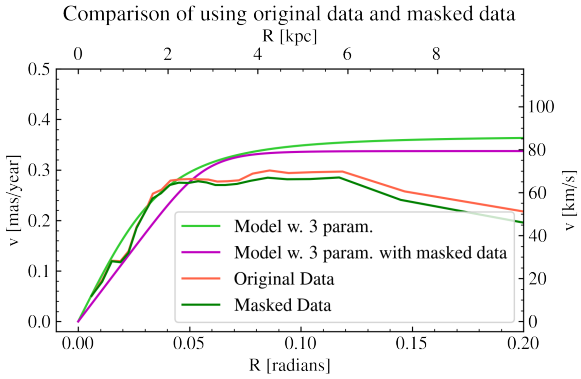

Figure A.20: The model with three parameters used with the masked and unmasked data for BL

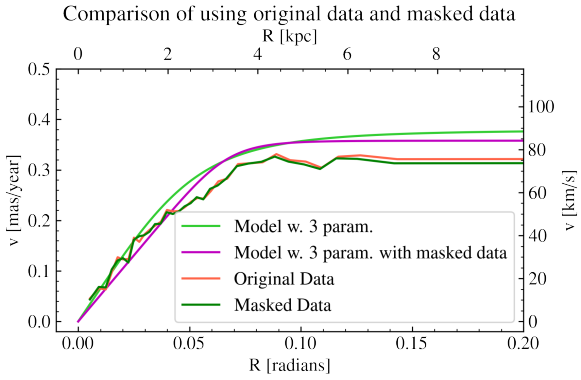

Figure A.21: The model with three parameters used with the masked and unmasked data for AGB

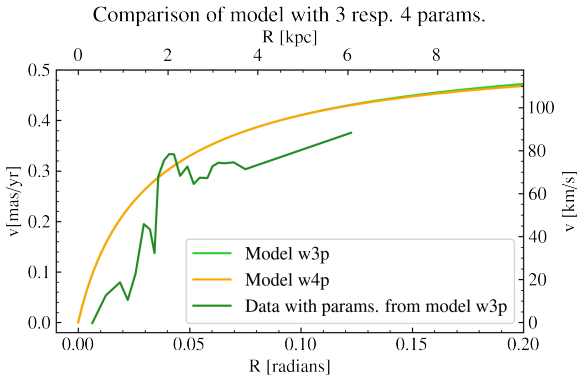

Figure A.22: Model with 3 parameters (w3p) compared to the model with 4 parameters (w4p) for Young 1. The data plotted using the parameters of the model with 3 parameters is indistinguishable from the data plotted using the parameters of the model with 4 parameters, so we only show one of these curves.

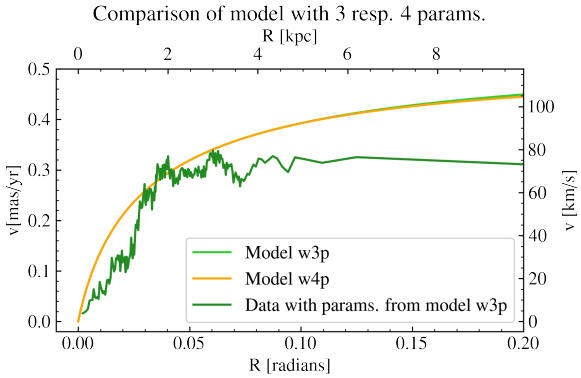

Figure A.23: Model with 3 parameters (w3p) compared to the model with 4 parameters (w4p) for Young 2. The data plotted using the parameters of the model with 3 parameters is indistinguishable from the data plotted using the parameters of the model with 4 parameters, so we only show one of these curves.

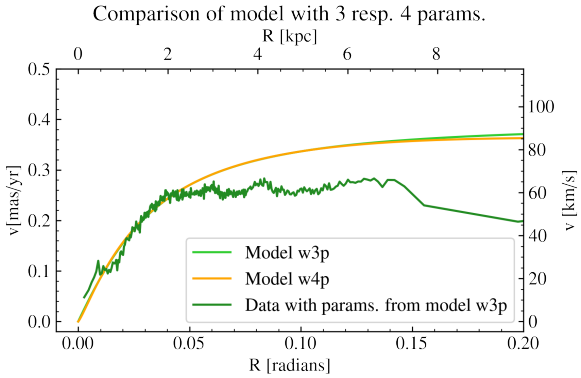

Figure A.24: Model with 3 parameters (w3p) compared to the model with 4 parameters (w4p) for Young 3. The data plotted using the parameters of the model with 3 parameters is indistinguishable from the data plotted using the parameters of the model with 4 parameters, so we only show one of these curves.

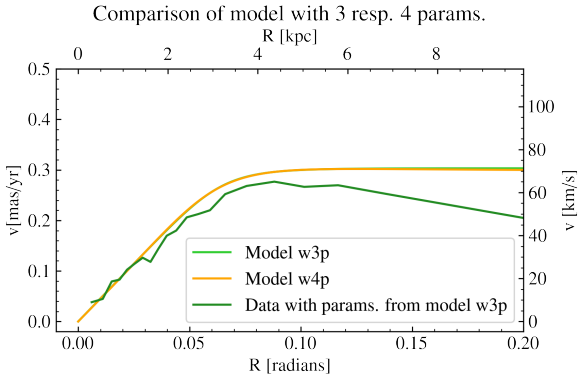

Figure A.25: Model with 3 parameters (w3p) compared to the model with 4 parameters (w4p) for RRL. The data plotted using the parameters of the model with 3 parameters is indistinguishable from the data plotted using the parameters of the model with 4 parameters, so we only show one of these curves.

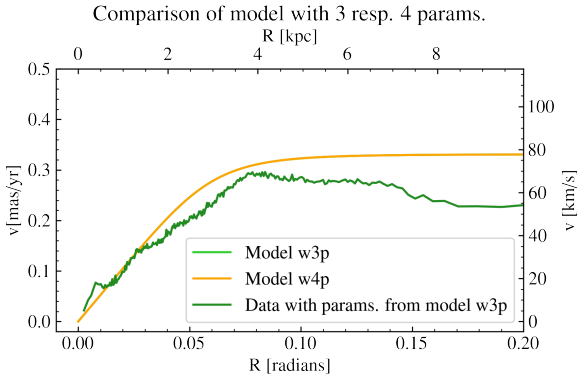

Figure A.26: Model with 3 parameters (w3p) compared to the model with 4 parameters (w4p) for RGB. The data plotted using the parameters of the model with 3 parameters is indistinguishable from the data plotted using the parameters of the model with 4 parameters, so we only show one of these curves.

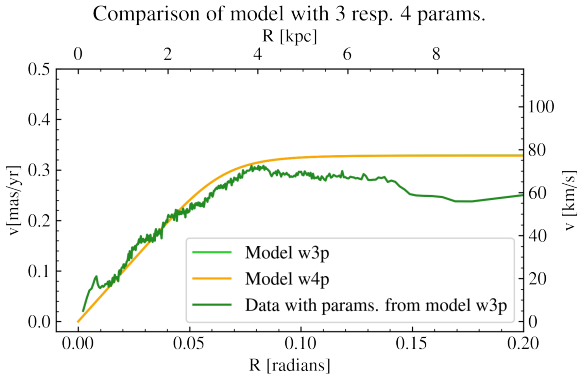

Figure A.27: Model with 3 parameters (w3p) compared to the model with 4 parameters (w4p) for RC. The data plotted using the parameters of the model with 3 parameters is indistinguishable from the data plotted using the parameters of the model with 4 parameters, so we only show one of these curves.

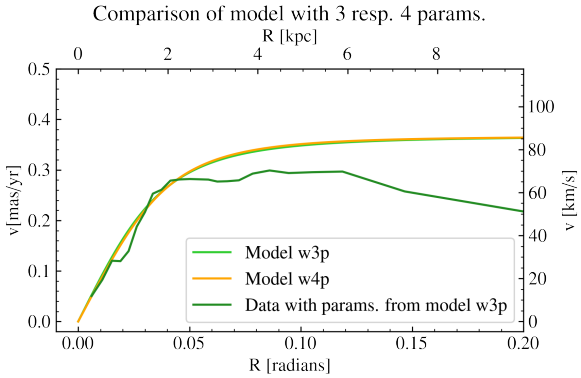

Figure A.28: Model with 3 parameters (w3p) compared to the model with 4 parameters (w4p) for BL. The data plotted using the parameters of the model with 3 parameters is indistinguishable from the data plotted using the parameters of the model with 4 parameters, so we only show one of these curves.

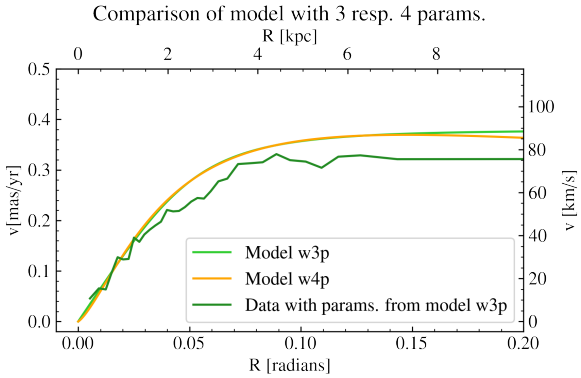

Figure A.29: Model with 3 parameters (w3p) compared to the model with 4 parameters (w4p) for AGB. The data plotted using the parameters of the model with 3 parameters is indistinguishable from the data plotted using the parameters of the model with 4 parameters, so we only show one of these curves.

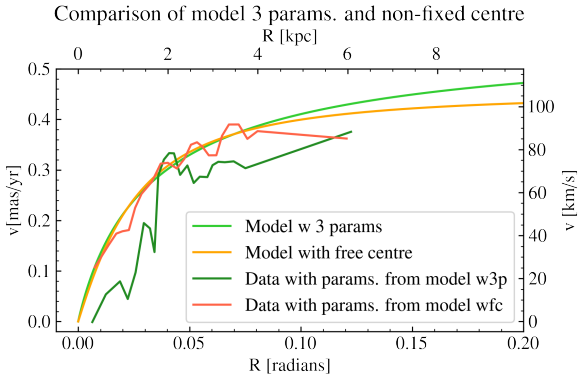

Figure A.30: Comparison of the rotation curve from the model with 3 parameters and the model with a free centre for Young 1.

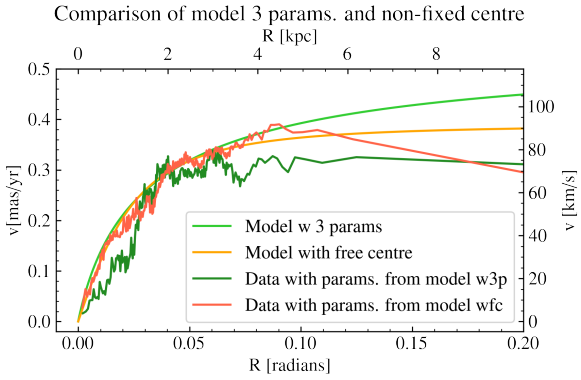

Figure A.31: Comparison of the rotation curve from the model with 3 parameters and the model with a free centre for Young 2.

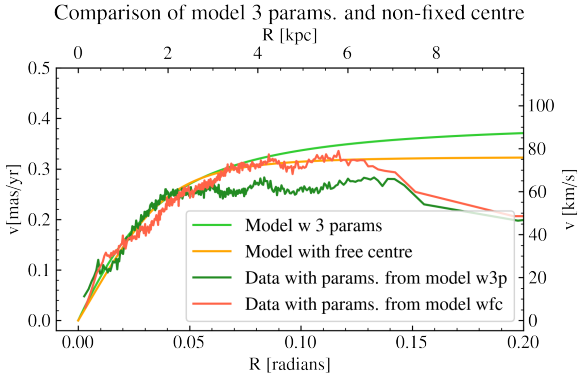

Figure A.32: Comparison of the rotation curve from the model with 3 parameters and the model with a free centre for Young 3.

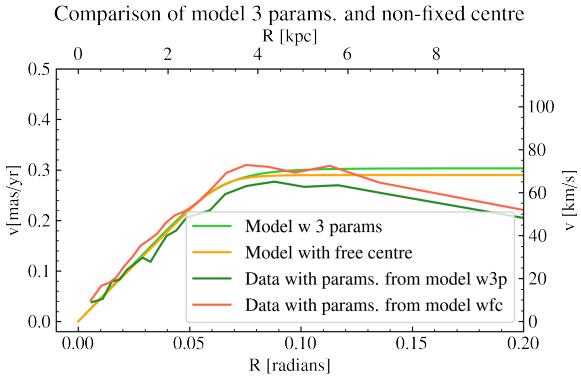

Figure A.33: Comparison of the rotation curve from the model with 3 parameters and the model with a free centre for RRL.

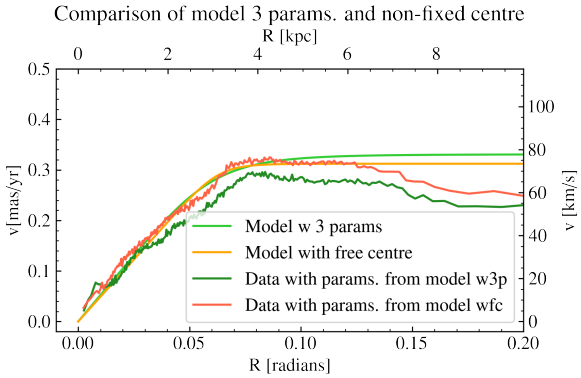

Figure A.34: Comparison of the rotation curve from the model with 3 parameters and the model with a free centre for RGB.

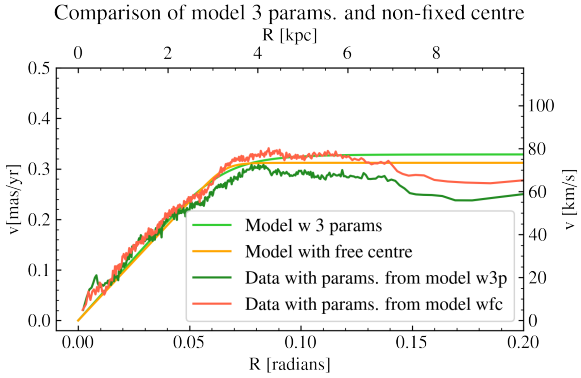

Figure A.35: Comparison of the rotation curve from the model with 3 parameters and the model with a free centre for RC.

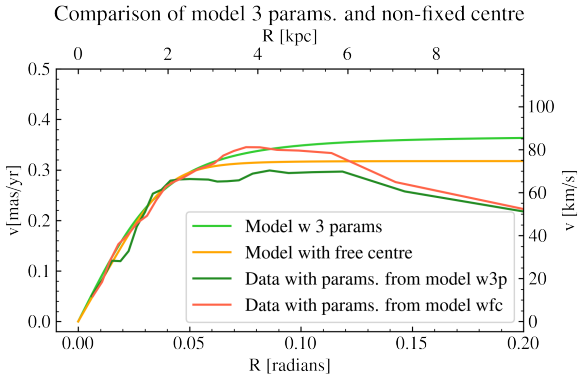

Figure A.36: Comparison of the rotation curve from the model with 3 parameters and the model with a free centre for BL.

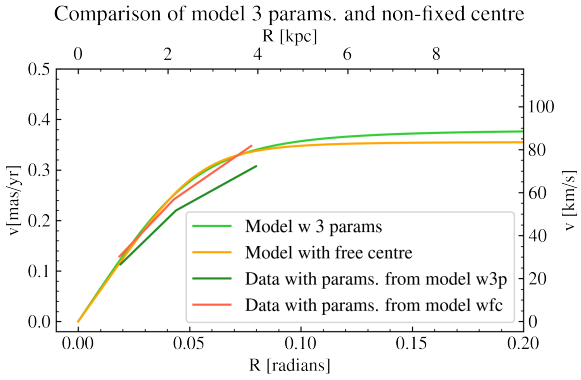

Figure A.37: Comparison of the rotation curve from the model with 3 parameters and the model with a free centre for AGB.

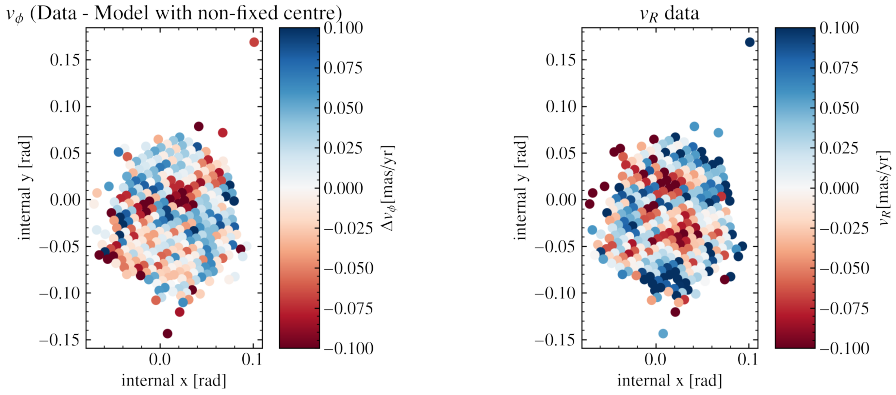

Figure A.38: Comparison between the data and the model with a non-fixed centre for the rotational and the radial velocity for the evolutionary phase Young 1.

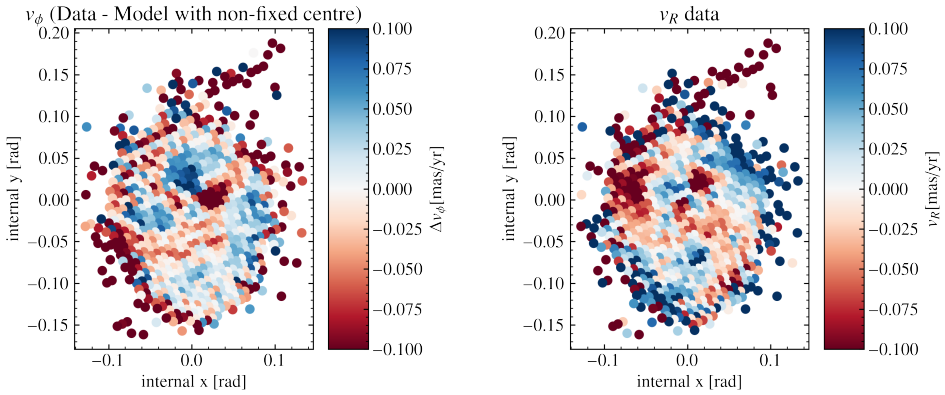

Figure A.39: Comparison between the data and the model with a non-fixed centre for the rotational and the radial velocity for the evolutionary phase Young 2.

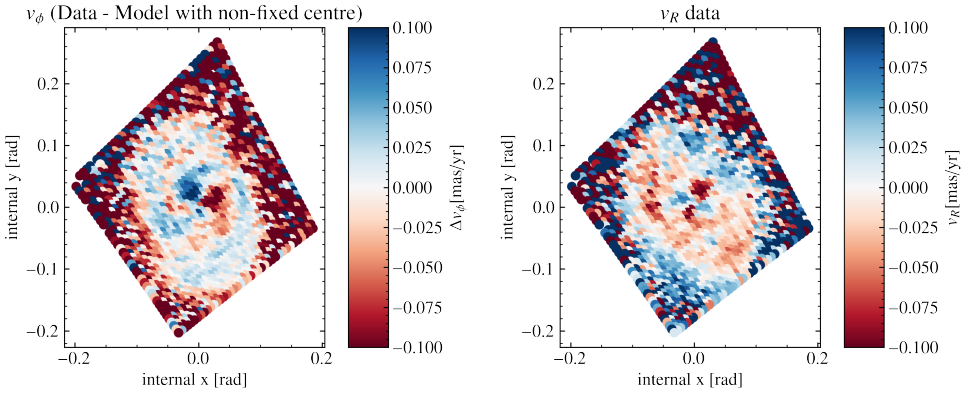

Figure A.40: Comparison between the data and the model with a non-fixed centre for the rotational and the radial velocity for the evolutionary phase Young 3.

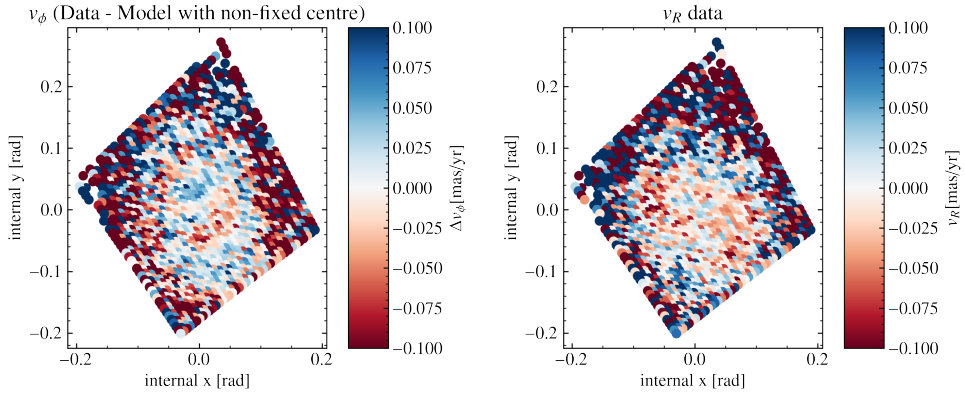

Figure A.41: Comparison between the data and the model with a non-fixed centre for the rotational and the radial velocity for the evolutionary phase RRL.

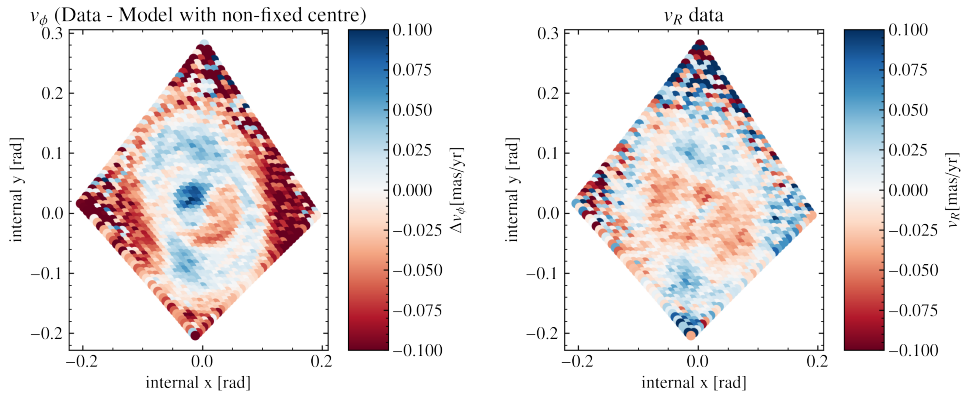

Figure A.42: Comparison between the data and the model with a non-fixed centre for the rotational and the radial velocity for the evolutionary phase RGB.

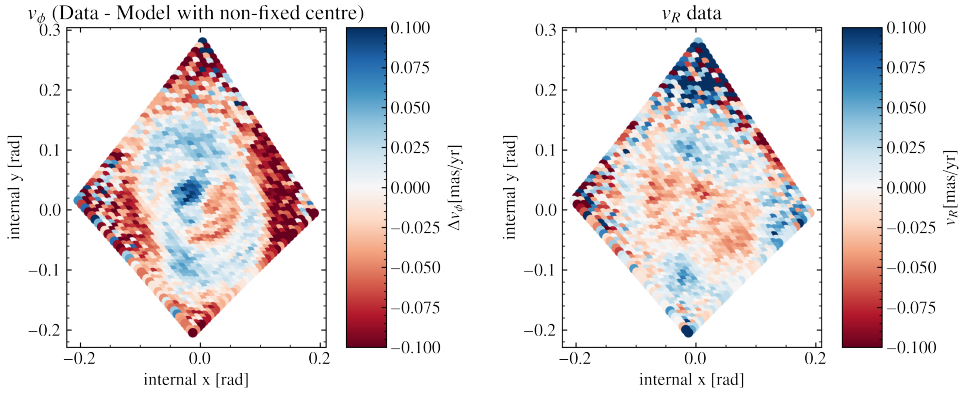

Figure A.43: Comparison between the data and the model with a non-fixed centre for the rotational and the radial velocity for the evolutionary phase RC.

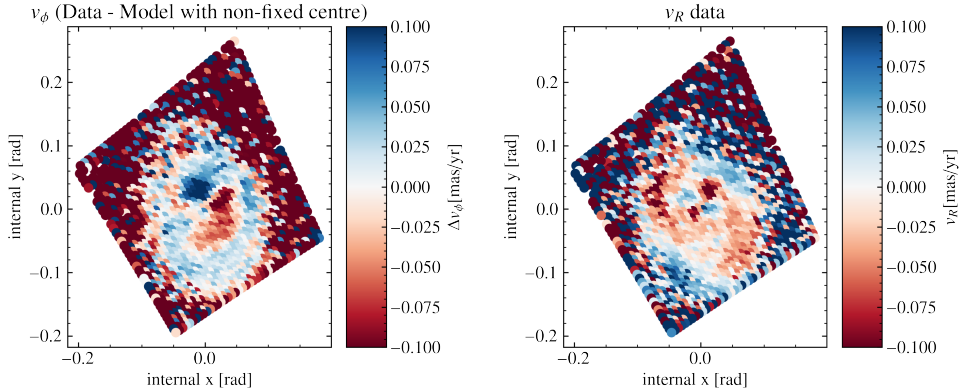

Figure A.44: Comparison between the data and the model with a non-fixed centre for the rotational and the radial velocity for the evolutionary phase BL.

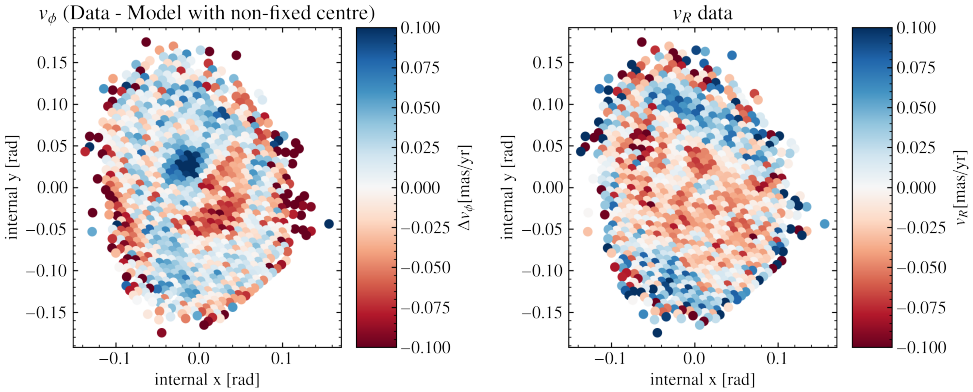

Figure A.45: Comparison between the data and the model with a non-fixed centre for the rotational and the radial velocity for the evolutionary phase AGB.